Late Cretaceous (81Ma) high-temperature metamorphism in the southeastern Lhasa terrane: implication for the Neo-Tethys ocean ridge subduction.

Journal Item

Tectonophysics xxx (2013) xxx–xxx

Contents lists available at ScienceDirect

Tectonophysics

journal homepage: www.elsevier.com/locate/tecto

Late Cretaceous (~81 Ma) high-temperature metamorphism in the southeastern Lhasa terrane: Implication for the Neo-Tethys ocean ridge subduction

Liang Guo [a,*], Hong-Fei Zhang [a,*], Nigel Harris [b], Fa-Bin Pan [a], Wang-Chun Xu [a]

[a] State Key Laboratory of Geological Processes and Mineral Resources and Faculty of Earth Sciences, China University of Geosciences, Wuhan 430074, China
[b] Department of Environment, Earth and Ecosystems, The Open University, Milton Keynes MK7 6AA, UK

ARTICLE INFO

Article history:
Received 8 April 2013
Received in revised form 9 October 2013
Accepted 11 October 2013
Available online xxxx

Keywords:
Eastern Himalayan syntaxis
Lhasa terrane
HT metamorphism
Ridge subduction
U–Pb zircon dating

ABSTRACT

An integrated study of U–Pb zircon dating, geochemical and Sr–Nd–Hf isotopic compositions of garnet-bearing granulite and marble from the granulite-facies domain of the Nyingchi Complex (eastern Himalayan syntaxis) has provided insights into the tectonic evolution of the southern Lhasa terrane. The peak metamorphism of the garnet-bearing granulite is marked by a mineral assemblage of garnet + orthopyroxene + high-Ti amphibole + plagioclase + quartz + rutile. Abundant exsolved rutile needles are observed within amphibole, garnet and quartz. The peak metamorphic temperatures are estimated at 803–924 °C. Geochemical data from the garnet-bearing granulites provide evidence for a basaltic protolith that formed in a continental-margin arc setting. Sr–Nd–Hf isotopic compositions indicate that this protolith was sourced from partial melting of a depleted mantle. LA-ICP MS U–Pb zircon dating shows that the protolith age and metamorphic age of the garnet-bearing granulites are 89.3 ± 0.6 Ma and 81.1 ± 0.8 Ma, respectively. The detrital magmatic zircons from the marble yield ages from 86.3 to 167 Ma. The age distribution and Hf isotopic composition ($\varepsilon_{Hf}(t)$ = +5.9 to +17.5) of the detrital magmatic zircon in the marble are consistent with the isotopic data of zircons from the Jurassic–Cretaceous Gangdese batholiths, suggesting that the clastic sediments were partially derived from these intrusives or associated volcanic rocks, and deposited in the fore-arc basin of the Gangdese arc. The metamorphic zircons in the marble yield a metamorphic age of 81.4 ± 0.5 Ma. These results show that both the arc magmatic rocks and forearc sedimentary rocks underwent high-temperature (HT) granulite-facies metamorphism at ~81 Ma, indicating anomalously high heat input in the forearc region. A range of tectonic observations, including a coeval hiatus in arc magmatism and a period of regional uplift, indicate that HT metamorphism resulted from the subduction of the Neo-Tethys ocean ridge beneath the southern Lhasa terrane during the Late Cretaceous.

1. Introduction

The subduction of an oceanic spreading ridge is likely to be a phenomenon that characterizes many convergent plate boundaries. Following ridge subduction, a slab window will form beneath the overriding plate as the plate growth along the diverging oceanic plate edges ceases (DeLong et al., 1979; Thorkelson, 1996). Ridge subduction and the associated slab window strongly affect the tectonic, metamorphic and magmatic evolution of the overriding plate (e.g., Aguillon-Robles et al., 2001; Brown, 1998; Cole and Stewart, 2009; DeLong et al., 1979; Groome and Thorkelson, 2009; Guillaume et al., 2010; Lagabrielle et al., 2000; Santosh and Kusky, 2010; Sisson et al., 2003; Thorkelson, 1996). Large porphyry Cu–Au deposits may be spatially associated with the oceanic ridge subduction (Haeussler et al., 1995; Sun et al., 2010). Importantly, the oceanic ridge subduction plays a pivotal role in crustal growth through the interaction between asthenospheric mantle and supracrustal rocks (Nelson and Forsythe, 1989; Tang et al., 2010). Identifying when ridge subduction has occurred is thus important for understanding the tectonic evolution of ancient convergent margins. Extensive studies of the effects of ridge subduction have been investigated in the modern Pacific Rim convergent margins (McCrory et al., 2009, and references therein). There are several geological effects related to the ridge subduction, including (1) adakitic rocks derived from partial melting of the oceanic crust at slab window edges (Tang et al., 2010; Thorkelson and Breitsprecher, 2005), and/or from partial melting of overlying lower crust (Cole et al., 2006); (2) a hiatus of arc magmatism due to the cessation of fluid-triggered mantle-wedge melting (Cole and Stewart, 2009, and references therein); (3) near-trench magmatism, either by decompression melting of

* Corresponding authors. Tel.: +86 27 67883003; fax: +86 27 67883002.
E-mail addresses: liangguocug@yahoo.com (L. Guo), hfzhang@cug.edu.cn (H.-F. Zhang).

0040-1951/$ – see front matter © 2013 Published by Elsevier B.V.
http://dx.doi.org/10.1016/j.tecto.2013.10.007

upwelling mantle, or from magmas derived from partial melting of the accretionary wedge sediments, or both (Bradley et al., 2003; Cole and Stewart, 2009; Cole et al., 2006; Marshak and Karig, 1977); (4) HT/UHT metamorphism in the fore-arc region (Brown, 1998; DeLong et al., 1979; Santosh and Kusky, 2010); (5) uplift of the fore-arc and arc region in response to the subduction of the topographic high and buoyant ridge, or the replacement of relatively cool lithospheric mantle by relatively hot asthenospheric mantle (Guillaume et al., 2009, 2010; Rogers et al., 2002); and (6) changes in structural style on either side of the slab window (Pavlis and Sisson, 1995). Although there is no unique signature of ridge subduction events, the observation of several of these features together can help identify regions where ridge subduction may have occurred in the past (Sisson et al., 2003). Near-trench magmatism and HT metamorphism are the most striking features attributable to ridge subduction, and are likely to be diagnostic of ancient ridge subduction (Brown, 1998; Santosh and Kusky, 2010).

The southern Lhasa terrane (Gangdese belt) was an Andean-type magmatic arc that resulted from the northward subduction of the Neo-Tethyan oceanic slab prior to the India–Asia collision (55 ± 10 Ma) (Allègre et al., 1984; de Sigoyer et al., 2000; Najman et al., 2010, and references therein; Yin and Harrison, 2000). The existing geochronological data indicate that the time of the Gangdese arc magmatism spans from late Triassic to Eocene (Chu et al., 2006; Ji et al., 2009; Lee et al., 2009; Schärer et al., 1984; Wen et al., 2008b; Xu et al., 1985). The closure of the Neo-Tethyan ocean would have involved at least one episode of spreading ridge subduction beneath the southern Lhasa terrane. Based on the occurrences of charnockite, adakitic rocks, and HT metamorphism, Zhang et al. (2010b, 2010c) and Meng et al. (2010) have suggested that a Late Cretaceous (~90 Ma) ridge subduction could have occurred in the southeastern Lhasa terrane. However, the presence of coeval (98–88 Ma) arc magmatic rocks conflict with the ridge subduction model (Guan et al., 2011). Guan et al. (2010) suggested instead that the ridge subducted at ~80 Ma based on the adakitic magmatism in the southeastern Lhasa terrane. The timing of ridge subduction therefore remains enigmatic.

Unlike the numerous igneous studies, the metamorphic history of southern Lhasa terrane is rarely studied (Booth et al., 2009; Guo et al., 2012; Harris et al., 1988; Wang et al., 2009; Zhang et al., 2010c). In the southeastern Lhasa terrane, the Nyingchi Complex underwent high temperature (HT) granulite-facies metamorphism (Geng et al., 2006; Zhang et al., 2010c). The ages of granulite-facies metamorphism and protolith of the Nyingchi Complex are important to understand the tectonic evolution of the active southern margin of Eurasia. Previous studies show that the metamorphic ages of the host rocks of the granulite are 80–90 Ma (Dong et al., 2012; Wang et al., 2009; Zhang et al., 2010c). However, the metamorphic age of the granulite remains uncertain. In addition, the age and origin of the protoliths of the granulites have not yet been well constrained. In this study, we focus on granulite facies rocks of the Nyingchi Complex and provide new evidence for Late Cretaceous (~81 Ma) forearc high-temperature (HT) metamorphism that resulted from the Neo-Tethys ocean ridge subduction. Our results, combined with studies on the igneous and tectonic history, provide new constraints on the Late Cretaceous evolution of the India–Asian collision.

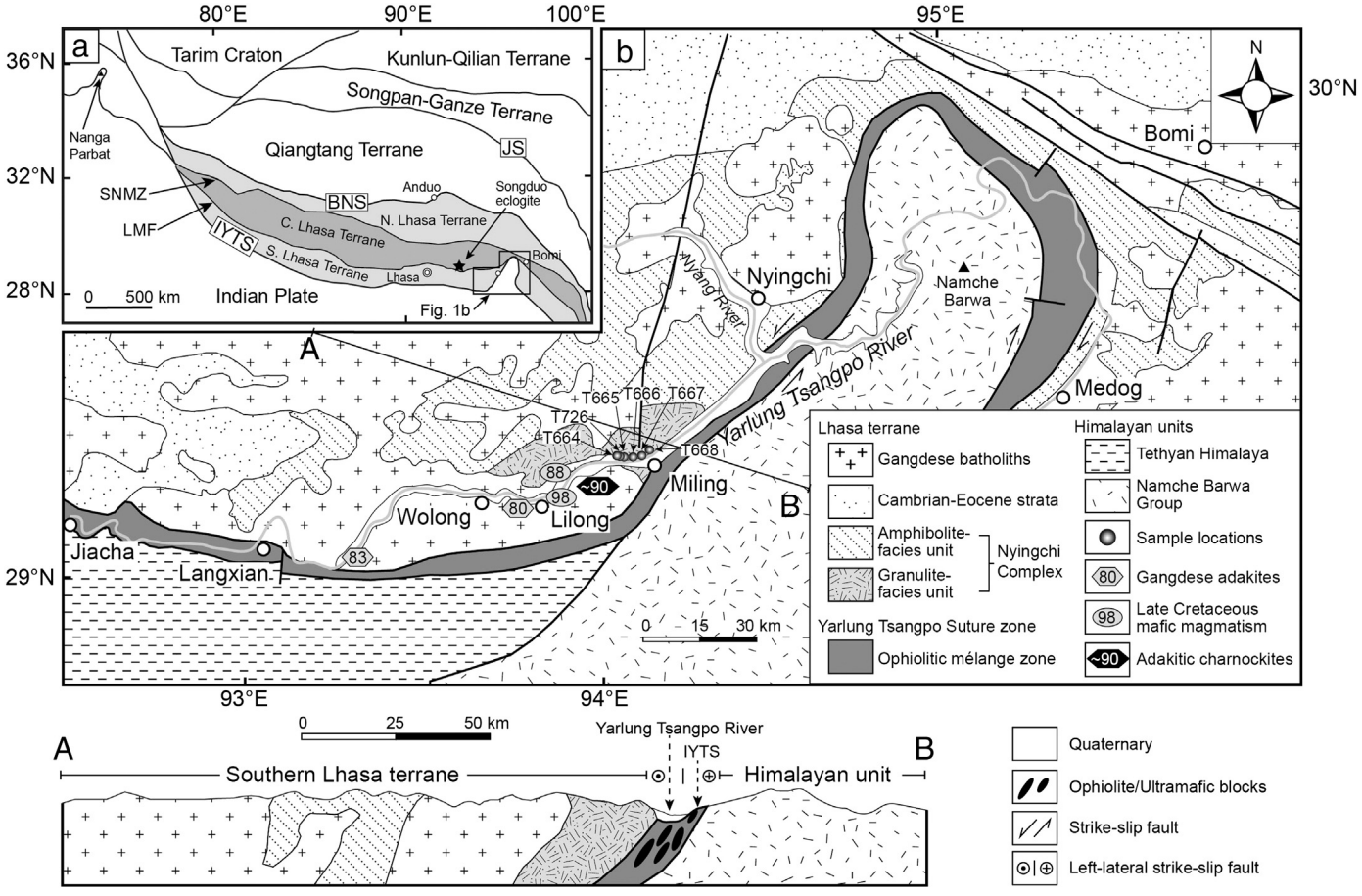

Fig. 1. (a) Tectonic framework of the Tibetan Plateau and the Lhasa terrane (modified from Zhu et al., 2011). JS = Jinsha Suture; BNS = Bangong–Nujiang Suture; SNMZ = Shiquan River–Nam Tso Mélange Zone; LMF = Luobadui–Milashan Fault; IYTS = Indus–Yarlung Tsangpo Suture. (b) Simplified geological map and cross-section of the eastern Himalayan syntaxis (modified from Zhang et al., 2010c), showing the locations of the studied samples and Late Cretaceous magmatism. The Late Cretaceous Gangdese adakities are from Wen et al., 2008a, mafic magmatism are from Guan et al., 2011, and adakitic charnockites are from Zhang et al., 2010b. All of the samples shown are of garnet-bearing granulite facies rocks with the exception of sample T668, which is from a marble unit contained in the granulite unit.

Please cite this article as: Guo, L., et al., Late Cretaceous (~81 Ma) high-temperature metamorphism in the southeastern Lhasa terrane: Implication for the Neo-Tethys ocean ridge subduction, Tectonophysics (2013), http://dx.doi.org/10.1016/j.tecto.2013.10.007

2. Geological background

The Tibetan Plateau is a collage of continental terranes that were accreted to the Eurasian plate during the Phanerozoic (Allègre et al., 1984; Dewey et al., 1988; Pan et al., 2012; Yin and Harrison, 2000). The Lhasa terrane is the southernmost terrane of the Asian continent (Fig. 1a), and is separated from the Qiangtang terrane to the north by the Bangong–Nujiang suture zone (BNS) and from the Tethyan Himalaya (Indian affinity) to the south by the Indus–Yarlung Tsangpo suture zone (IYTS) (Dewey et al., 1988; Pan et al., 2012). Based on contrasting sedimentary covers, it can be divided into northern, central, and southern Lhasa terranes (Fig. 1a), separated by the Shiquan River–Nam Tso Mélange Zone (SNMZ) and Luobadui–Milashan Fault (LMF), respectively (Zhu et al., 2011). The northern Lhasa terrane is mainly covered by Jurassic–Cretaceous volcanic rocks, which were intruded by Mesozoic (130–80 Ma) plutonic rocks (Zhu et al., 2009a, and references therein). The central Lhasa terrane comprises Precambrian basement (e.g. the Nyainqentanglha gneisses), overlain by Paleozoic–Cretaceous sedimentary cover (Hu et al., 2005; Zhu et al., 2011). The southern Lhasa terrane is dominated by Cretaceous–Early Tertiary Gangdese batholiths and the Linzizong volcanic succession (Chu et al., 2006; Coulon et al., 1986; Ji et al., 2009; Lee et al., 2009; Wen et al., 2008b; Zhang et al., 2007). There is an apparent hiatus in Gangdese arc magmatism in the southern Lhasa terrane between 80 and 70 Ma, the cause of which remains unclear (Volkmer, 2010; Wen et al., 2008b). Wen et al. (2008a, 2008b) attributed it to a brief episode of shallow-subduction. Volkmer (2010) suggested that the formation of eclogitic lithospheric root resulted from shortening of Gangdese arc that caused the lull in magmatic activity. Regionally, the 69–40 Ma Linzizong volcanic rocks in the Gangdese unconformably overlie strongly deformed Late Cretaceous and/or older rocks (Burg and Chen, 1984; England and Searle, 1986; Kapp et al., 2007; Leier et al., 2007), suggesting that significant crustal shortening and uplift occurred prior to 69 Ma. The Xigaze fore-arc basin is located at the southern margin of the southern Lhasa terrane, immediately north of the Yarlung–Tsangpo suture zone, extends from Xigaze in the east to Saga in the west with a length of ~550 km (west of our study area). This basin is mainly composed of Late Cretaceous coarse- to fine-grained volcaniclastic sedimentary rocks, with minor intercalated hemi-pelagic marl (Dürr, 1996; Einsele et al., 1994). Previous studies indicated that the clastic sediments mainly sourced from the Gangdese arc (Dürr, 1996; Einsele et al., 1994; Wu et al., 2010).

In the eastern Himalayan syntaxis, the southern Lhasa terrane is separated from the Himalayan unit by the Yarlung–Tsangpo suture zone (Fig. 1b). In the Yarlung–Tsangpo suture zone, the ultramafic and mafic blocks coexist with blastobasalt pillow lava and quartzite to form relatively complete ophiolitic sequence (Geng et al., 2006). Zircon U–Pb geochronology studies suggested that the ophiolite formed in early Jurassic and locally in Late Triassic (Geng et al., 2011). The geochemical studies on the metamorphic mafic rocks of the ophiolite indicated that the Neo-Tethyan Ocean involved a two-stage evolution: (1) initial formation by melting of MORB-OIB mantle source; and (2) entrapment within the mantle above a subduction zone (Geng et al., 2010).

In the southeastern Lhasa terrane, as exposed along the western margin of the eastern syntaxis, there is no residual fore-arc basin between the southern Lhasa terrane and Yarlung–Tsangpo suture zone. The southern Lhasa terrane mainly consists of granitic plutons intruding the high-grade Nyingchi Complex and Cambrian–Eocene strata (Fig. 1b) (Geng et al., 2006; Guo et al., 2012; Zhang et al., 2008). The Nyingchi Complex and granitic plutons are directly contact with the Yarlung–Tsangpo suture zone (Fig. 1b). The granitic plutons have been dated from 165 to 22 Ma (Guan et al., 2010; Guo et al., 2011, 2012; Wen et al., 2008a; Zhang et al., 2008, 2010a, 2010b), similar to those of the Gangdese batholiths in the central part of the southern Lhasa terrane (Chu et al., 2006; Ji et al., 2009; Wen et al., 2008b; Zhang et al., 2007). The Late Cretaceous intrusions are well developed in the western margin of the eastern syntaxis. For example, the Wolong pluton (83–80 Ma) exhibits adakitic geochemical characteristics, resulting from partial melting of the underplated basaltic lower crust (Guan et al., 2010; Wen et al., 2008a). Zhang et al. (2010b) and Guan et al. (2011) reported a suite of Late Cretaceous (90–88 Ma) charnockite and a suite of Late Cretaceous (98–88 Ma) mafic rocks in Lilong area, respectively. In addition, Guo et al. (2011) reported a ~80 Ma gneissic

Table 1
Geochemical data of the garnet-bearing granulites from the Nyingchi Complex.

Sample	T664	T665	T666	T667	T726
Latitude	N29°12′ 20.8″	N 29°12′ 19.1″	N 29°12′ 14.8″	N29°12′0.7″	N29°12′ 21.0″
Longitude	E94°07′ 10.4″	E 94°07′ 16.6″	E 94°07′ 27.0″	E 94°08′ 32.6″	E94°07′ 10.3″
(wt.%)					
SiO_2	51.81	50.71	52.83	54.65	54.1
TiO_2	0.97	0.81	0.78	0.78	0.97
Al_2O_3	18.68	19.54	19.12	18.14	16.73
TFe_2O_3	11.55	9.53	8.66	8.66	11.48
MnO	0.19	0.15	0.13	0.14	0.22
MgO	4.02	4.81	4.5	4.27	2.85
CaO	7.04	8.59	8.05	7.78	9.23
Na_2O	3.39	3.96	4.12	3.33	2.99
K_2O	1.33	0.59	0.82	1.05	0.49
P_2O_5	0.3	0.25	0.19	0.21	0.22
Loi	0.9	1.46	1.26	1.31	0.74
Tol	100.18	100.4	100.46	100.32	100.02
Mg#	41	50	51	49	33
(ppm)					
Sc	21.2	19.6	20.6	19.0	26.6
V	259	219	211	213	248
Cr	13.3	23.2	15.2	25.9	1.41
Co	69.5	47.4	49.0	51.7	64.1
Ni	15.3	19.1	16.1	22.8	4.40
Cu	72.9	45.1	20.0	88.8	110
Zn	110	89.7	88.7	83.4	91.2
Ga	20.6	19.9	19.7	19.2	19.5
Rb	38.2	6.73	10.6	21.1	8.43
Sr	616	627	629	586	678
Y	21.8	17.2	16.4	15.4	28.1
Zr	20.8	18.6	21.7	21.5	32.8
Nb	2.88	1.89	2.24	2.12	2.44
Ba	256	177	168	295	99.8
La	11.0	9.30	9.30	9.44	11.2
Ce	25.9	21.1	21.4	20.1	25.4
Pr	3.62	2.79	2.87	2.54	3.51
Nd	17.3	12.8	12.9	11.4	15.9
Sm	4.09	3.02	3.11	2.76	4.19
Eu	1.25	1.01	0.98	1.02	1.22
Gd	4.01	2.96	2.99	2.72	4.33
Tb	0.61	0.48	0.48	0.43	0.75
Dy	3.82	3.01	2.78	2.66	4.75
Ho	0.75	0.60	0.56	0.52	0.98
Er	2.18	1.71	1.64	1.56	2.88
Tm	0.33	0.25	0.23	0.22	0.44
Yb	2.08	1.63	1.45	1.45	2.78
Lu	0.32	0.24	0.22	0.23	0.41
Hf	0.77	0.76	0.93	0.81	1.21
Ta	0.32	0.20	0.26	0.26	0.30
Pb	7.11	7.04	10.1	10.8	9.17
Th	0.864	0.46	1.19	1.55	2.25
U	0.218	0.16	0.38	0.53	0.51
$(La/Yb)_N$	3.8	4.1	4.6	4.7	2.9
$^{87}Sr/^{86}Sr$	0.704765		0.704394	0.704502	0.704607
$(^{87}Sr/^{86}Sr)_i$	0.70454		0.70433	0.70437	0.70456
$^{143}Nd/^{144}Nd$	0.512776		0.512812	0.512845	0.512753
$(^{143}Nd/^{144}Nd)_i$	0.512693		0.512727	0.512759	0.512660
$\varepsilon_{Nd}(t)$	3.3		4.0	4.6	2.7
T_{DM} (Ga)	0.80		0.76	0.69	1.12

Notes: LOI = Loss on ignition; TFe_2O_3 = All Fe calculated as Fe_2O_3; Mg# = 100(Mg/Mg + Fe).

Please cite this article as: Guo, L., et al., Late Cretaceous (~81 Ma) high-temperature metamorphism in the southeastern Lhasa terrane: Implication for the Neo-Tethys ocean ridge subduction, Tectonophysics (2013), http://dx.doi.org/10.1016/j.tecto.2013.10.007

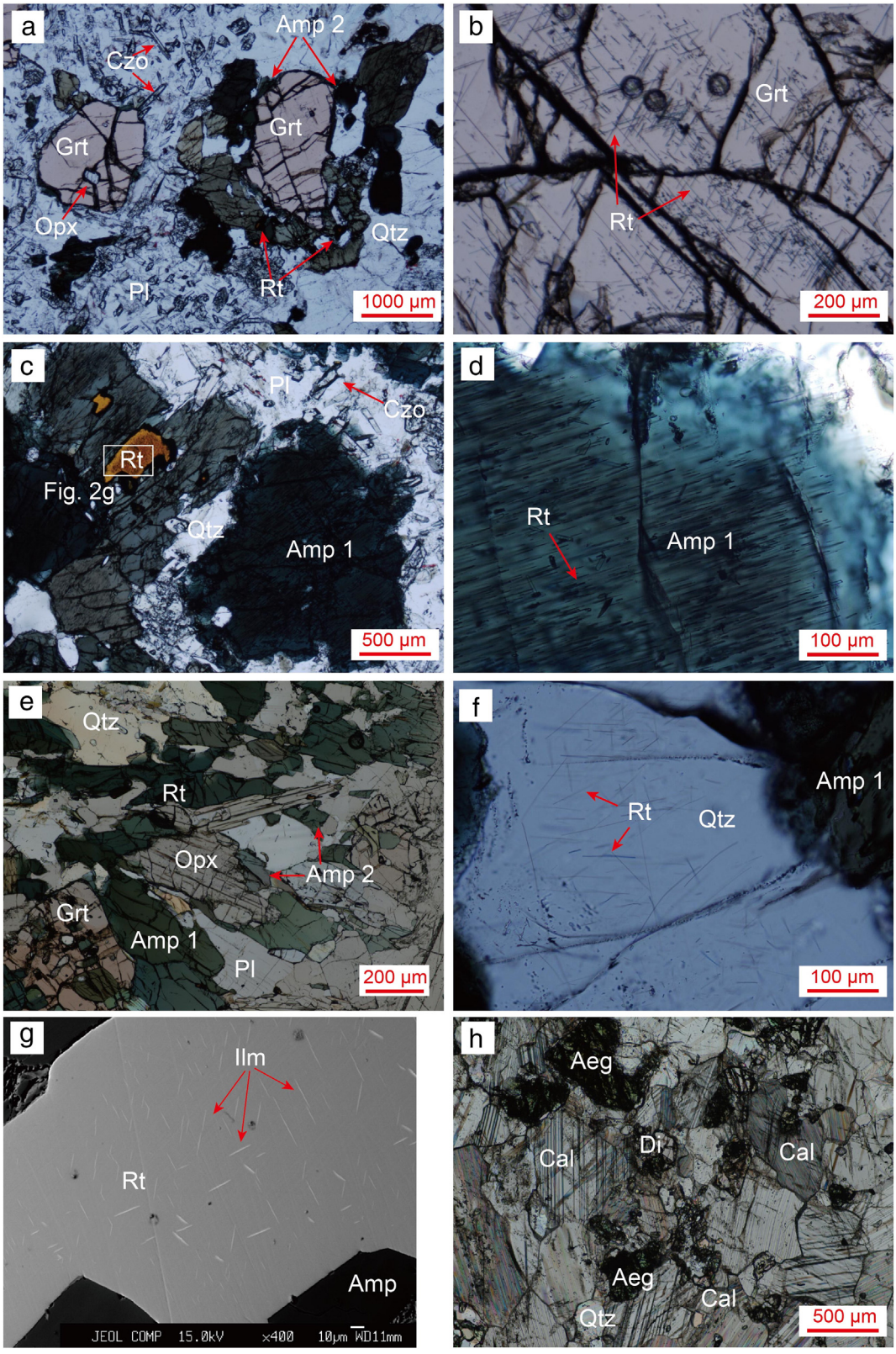

Fig. 2. Photomicrographs for the garnet-bearing granulite (a–g) and the marble (h) from the Nyingchi Complex in the eastern Himalayan syntaxis. (a) The porphyroblast garnet is partially replaced by retrograde symplectites of amphibole + plagioclase + rutile (sample T666). Garnet contains orthopyroxene inclusion. (b) Oriented rutile needles in garnet (sample T666). (c) The type 1 amphibole containing rutile inclusions (sample T664). (d) Core–rim structure from type 1 amphibole (sample T664). (e) Orthopyroxene partially replaced by type 2 amphibole (sample T667). (f) Oriented rutile needles in quartz (sample T666). (g) Oriented ilmenite needles in rutile (sample T664, backscattered electron image). (h) Calcite, diopside, aegirine and quartz assemblage from the marble (sample T668). Abbreviations: Aeg = aegirine; Amp = amphibole; Cal = calcite; Czo = clinozoisite; Di = diopside; Grt = garnet; Ilm = ilmenite; Opx = orthopyroxene; Pl = plagioclase; Qtz = quartz; Rt = rutile.

Please cite this article as: Guo, L., et al., Late Cretaceous (~81 Ma) high-temperature metamorphism in the southeastern Lhasa terrane: Implication for the Neo-Tethys ocean ridge subduction, Tectonophysics (2013), http://dx.doi.org/10.1016/j.tecto.2013.10.007

granite resulting from magma mixing between juvenile and old crustal materials.

The Nyingchi Complex, to the north of the Yarlung–Tsangpo suture zone (Fig. 1b), was considered to be the Precambrian basement of the Lhasa terrane based on the middle- and high-grade metamorphism (Geng et al., 2006). However, the detrital zircon U–Pb dating shows that the metasedimentary rocks from the Nyingchi Complex are no older than 490 or 340 Ma (Dong et al., 2010; Guo et al., 2012; Zhang et al., 2008). Due to the lack of detailed geological and geochemical investigation, the age and origin of the protoliths of the Nyingchi Complex have not yet been well documented. The existing studies show that the Nyingchi Complex is a set of tectonic mélange involved in different ages and various lithologies (Dong et al., 2010; Guo et al., 2011, 2012; Zhang et al., 2008, 2010c). The Nyingchi Complex can be divided into granulite-facies and amphibolite-facies metamorphic units (Fig. 1b) (Zhang et al., 2010c). The granulite-facies metamorphic unit is composed of granulite, garnet-bearing amphibolite and marble. The granulite occurs as lenses or blocks within the amphibolite-facies country rocks. The amphibolite-facies metamorphic unit consists of migmatite, amphibolitic gneiss, granitic gneiss, kyanite–sillimanite biotite schist and marble (Booth et al., 2009; Guo et al., 2011, 2012; Zhang et al., 2008, 2010c). The *P–T* conditions for the granulite-facies and amphibolite-facies have been estimated at 0.9–1.3 GPa, 830–900 °C and 0.8–1.2 GPa, 600–800 °C, respectively (Booth et al., 2009; Wang et al., 2009; Zhang et al., 2010c).

3. Petrography

Five garnet-bearing granulite samples (T664, T665, T666, T667, and T726) and a marble sample (T668) of this study have been collected from the granulite facies unit of the Nyingchi Complex (Zhang et al., 2010c) (Fig. 1b). Outcrop GPS coordinates for the garnet-bearing granulite samples are given in Table 1. Because of the thick soil cover, the field relations between the garnet-bearing granulite and marble are unexposed.

3.1. Garnet-bearing granulite

All five garnet-bearing granulite samples display porphyroblastic texture and gneissose structure. They have similar mineral assemblages, and consist of garnet, amphibole, plagioclase, orthopyroxene, quartz, clinozoisite, epidote, rutile, ilmenite, and zircon (Fig. 2a–g). Based on the mineral assemblages and microstructures, two metamorphic stages are recognized: peak granulite facies and retrograde amphibolite facies. All the samples have undergone retrograde metamorphism, and locally preserve relics of the peak metamorphic assemblages.

The garnets from all the five samples occur as subhedral to euhedral porphyroblasts, with a grain size of 1–5 mm. The garnet porphyroblasts in sample T666 contain inclusions of orthopyroxene, quartz and rutile (Fig. 2a). Most garnet grains contain exsolved needles of rutile (Fig. 2b). The garnet porphyroblasts are partially replaced by fine-grained symplectites (Fig. 2a). The symplectites are composed of amphibole and plagioclase, with or without rutile (Fig. 2a). Amphibole can be divided into two types based on their mode and composition. Type 1 consists of relatively large grains (up to 3 mm) and contains a large number of rutile exsolution needles (Fig. 2c–e), suggesting their high-Ti precursors. Some Type 1 amphiboles in sample T664 show core–rim structure, and the mineral color changes from brownish in the core to greenish in the rim (Fig. 2d). Type 2 consists of a greenish and fine-grained

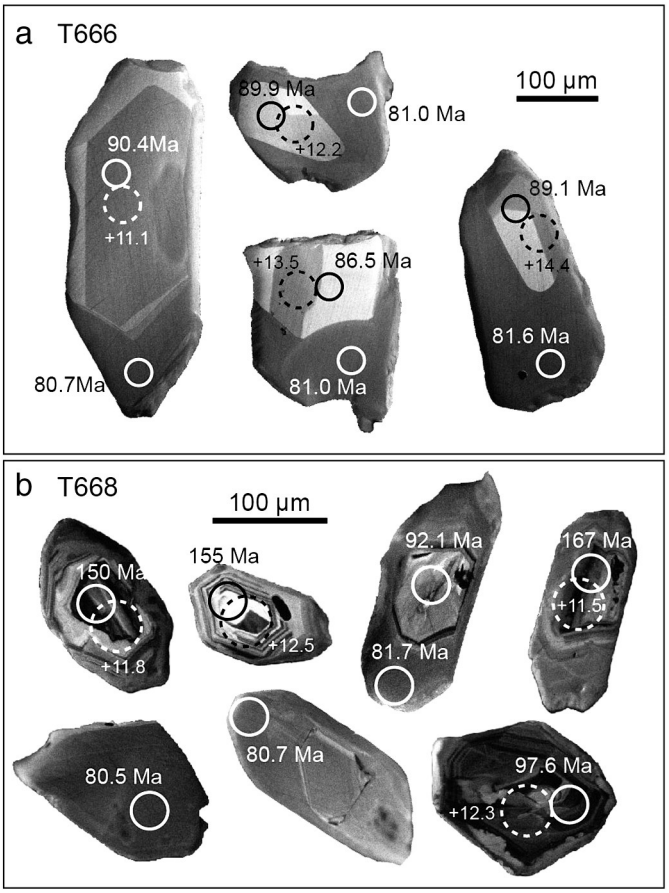

Fig. 3. Typical zircon CL images for (a) the garnet-bearing granulite and (b) the marble. The smaller circles show LA-ICP MS dating spots and corresponding U–Pb ages (in Ma), the dashed circles show locations of Lu–Hf isotope analysis and corresponding $\varepsilon_{Hf}(t)$ values.

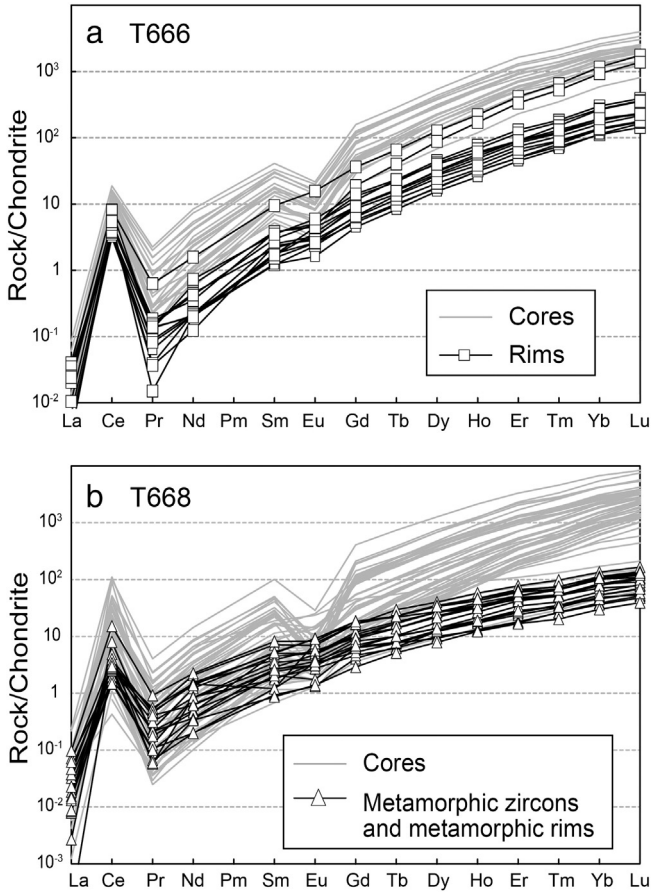

Fig. 4. Chondrite-normalized REE patterns of the zircons from (a) the garnet-bearing granulite and (b) the marble. Chondrite normalization values from Sun and McDonough (1989).

Please cite this article as: Guo, L., et al., Late Cretaceous (~81 Ma) high-temperature metamorphism in the southeastern Lhasa terrane: Implication for the Neo-Tethys ocean ridge subduction, Tectonophysics (2013), http://dx.doi.org/10.1016/j.tecto.2013.10.007

aggregate with plagioclase (Fig. 2a). The Orthopyroxene granis form two morphological types. The large anhedral orthopyroxenes in sample T667 are generally replaced by greenish amphibole (Fig. 2e). The fine-grained orthopyroxenes are mainly included in the garnet porphyroblasts (Fig. 2a). Clinozoisite and epidote occur as the alteration product of plagioclase, mainly within the plagioclase along the cleavage (Fig. 2a, c). Two generations of rutile are identified in sample T664, T665, T666, and T726. The first generation is seen as dark brown to black single crystal inclusions within amphibole, garnet, or quartz grains (Fig. 2a, c). Some rutile grains in sample T664 contain regular ilmenite exsolution lamellae (Fig. 2g), indicating that they have significant Fe content (Banfield and Veblen, 1991; Zack et al., 2004). The second generation occurs as exsolution needles within garnet, quartz and amphibole (Fig. 2b, d, f). The rutile needles in garnets and quartz are distributed along three crystallographically oriented planes (Fig. 2b, f). Most needles are 100–200 μm in length and <1 μm in diameter (Fig. 2b, f). The rutile needles in amphibole are 50–200 μm in length and 1–5 μm in diameter, and distribute along one or two crystallographically oriented planes (Fig. 2d). These rutile needles within garnet, hornblende and quartz are thought to be formed by

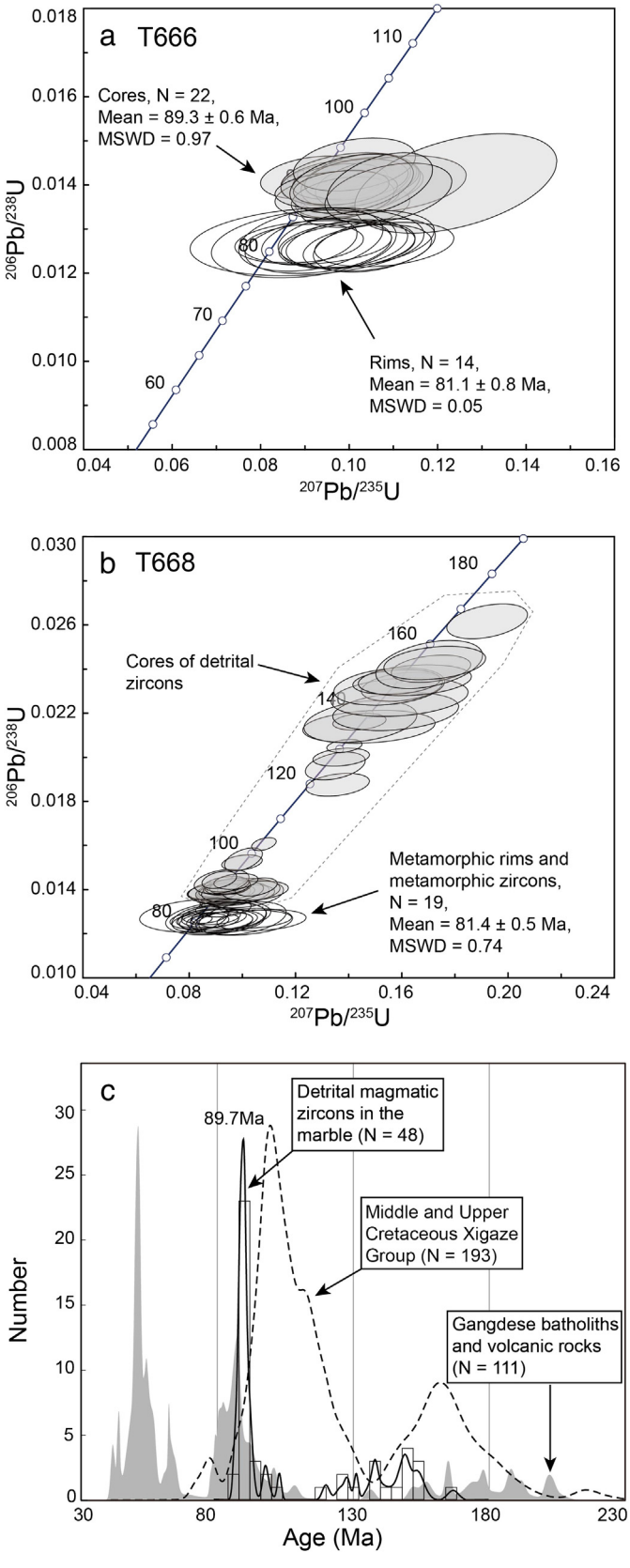

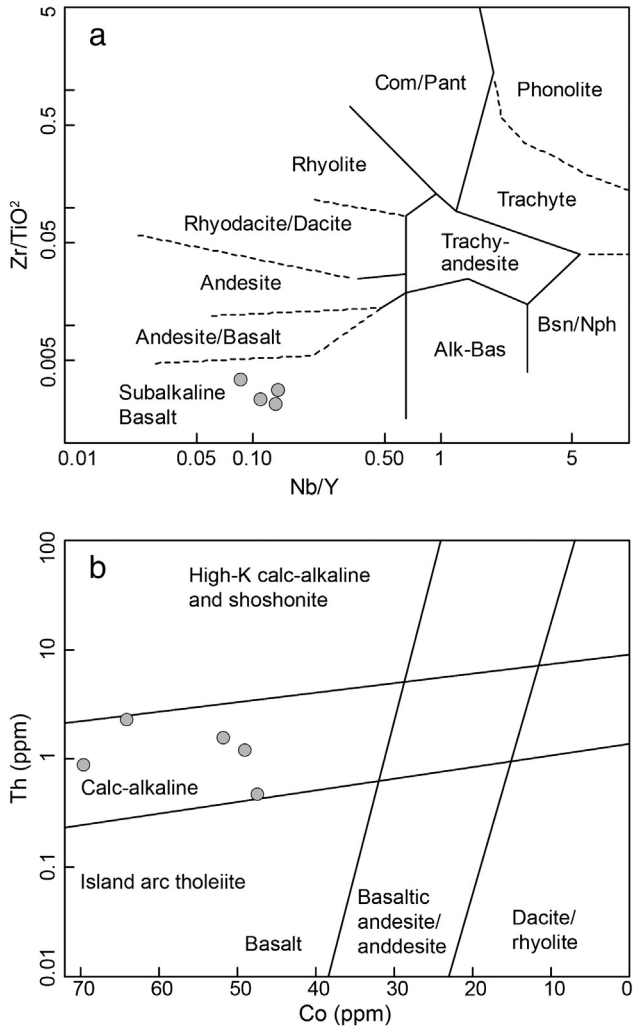

Fig. 6. Geochemical classification for the garnet-bearing granulite in the southern Lhasa terrane in the eastern Himalayan syntaxis. (a) Zr/TiO_2 – Nb/Y diagram of Winchester and Floyd (1977); (b) Th – Co plot of Hastie et al. (2007).

Fig. 5. U – Pb concordia diagrams for the zircon from (a) the garnet-bearing granulite and (b) the marble from the Nyingchi Complex. (c) The relative probability and frequency plots of the U – Pb ages of detrital magmatic zircon from the marble. Also plotted for comparison, the relative probability diagram of zircon U – Pb ages of the Late Triassic–Eocene Gangdese batholiths and volcanic rocks (in gray) (Chu et al., 2006; Guan et al., 2010, 2011; Guo et al., 2011, 2012; Ji et al., 2009; Jiang et al., 2012; McDermid et al., 2002; Quidelleur et al., 1997; Wen et al., 2008a, 2008b; Zhang et al., 2007, 2010b; Zhu et al., 2008, 2009a, 2009b, 2011), and the detrital zircon age spectra for the Middle–Upper Cretaceous Xigaze forearc sedimentary rocks (in dashed line) (Aitchison et al., 2011; Wu et al., 2010).

Please cite this article as: Guo, L., et al., Late Cretaceous (~81 Ma) high-temperature metamorphism in the southeastern Lhasa terrane: Implication for the Neo-Tethys ocean ridge subduction, Tectonophysics (2013), http://dx.doi.org/10.1016/j.tecto.2013.10.007

titanium exsolution during cooling, and suggest that titanium is saturated in these minerals during prograde metamorphism (Adachi et al., 2010; Kawasaki and Osanai, 2008; Thomas et al., 2010; Wark and Watson, 2006).

In summary, the garnet-bearing granulites from Nyingchi Complex experienced an early stage of granulite-facies metamorphism and a late stage of amphibolite-facies retrogression. The peak granulite-facies is characterized by a mineral assemblage of garnet + orthopyroxene + high-Ti amphibole + plagioclase + quartz + rutile. The retrograde amphibolite facies is represented by a mineral assemblage of plagioclase + low-Ti amphibole + quartz + rutile.

3.2. Marble

Primary compositional layers with distinct color bands are partially preserved in thick marble beds. The grayish-green marble layers are rich in silicate minerals whereas the white marble layers contain nearly pure carbonate. The marble sample T668 (N29°12′31.6″, E94°10′7.3″) is grayish-green in color. It shows blastic texture and massive structure, and mainly consists of calcite, and minor diopside, aegirine, quartz and tremolite (Fig. 2h).

4. Analytical methods

4.1. Zircon trace elements and U–Pb dating

Zircons were separated from rock samples using conventional heavy liquid and magnetic separation techniques. Cathodoluminescence (CL) images, taken at Northwest University (China), were used to check the internal structures of individual zircon grains and to guide U–Pb dating and Hf isotope analysis. Zircon U–Pb isotopic analyses were conducted by laser-ablation, inductively coupled plasma mass spectrometer (LA–ICP–MS) at the State Key Laboratory of Geological Processes and Mineral Resources (GPMR), China University of Geosciences. Laser sampling was performed using a GeoLas 2005. An Agilent 7500a ICP–MS instrument was used to acquire ion-signal intensities. Helium was applied as a carrier gas. Argon was used as the make-up gas and mixed with the carrier gas via a T-connector before entering the ICP. Nitrogen was added into the central gas flow (Ar + He) of the Ar plasma to decrease the detection limit and improve precision (Hu et al., 2008). Each analysis incorporated a background acquisition of approximately 20–30 s (gas blank) followed by 50 s data acquisition from the sample. The Agilent Chemstation was utilized for the acquisition of each individual analysis. A beam diameter of 32 μm was used. Zircon 91500 was used as an external standard and the NIST610 glass was used as an external standard. Detailed operating conditions for the laser ablation system and the ICP–MS instrument and data reduction are the same as described by Liu et al. (2010a, 2010b). Off-line selection and integration of background and analyte signals, and time-drift correction and quantitative calibration were conducted by ICPMSDataCal (Liu et al., 2010a). We use $^{206}Pb/^{238}U$ ages for zircons <1000 Ma and $^{207}Pb/^{206}Pb$ ages for zircons >1000 Ma. The data were processed using the ISOPLOT program of Ludwig (2003). The analytical data of zircon U–Pb dating and trace elements are give in Appendix Tables A1 and A2, respectively.

4.2. Zircon Lu–Hf isotope

In situ zircon Lu–Hf isotopic measurements were performed on the dated zircons using the LA–MC–ICPMS, at Northwest University in Xi'an. Analytical spots were located close to or on the top of LA–ICPMS spots or in the same growth domain as inferred from CL images. The analytical protocol used was similar to that outlined in Yuan et al. (2008). The analyses were undertaken using a spot size of 44 μm, an 8 Hz repetition rate and a laser power of 100 mJ/pulse. Zircon 91500, GJ-1 and Monastery were used as the reference standard. The decay constant for ^{176}Lu and the chondritic ratios of $^{176}Hf/^{177}Hf$ and $^{176}Lu/^{177}Hf$ used in calculations are 1.865×10^{-11}/year (Scherer et al., 2001), and 0.282772 and 0.0332 (Blichert-Toft and Albarede, 1997), respectively. The single-stage model age (T_{DM1}) was calculated relative to the depleted mantle with a present-day $^{176}Hf/^{177}Hf$ ratio of 0.28325 and $^{176}Lu/^{177}Hf$ ratio of 0.0384 (Griffin et al., 2000), and two-stage model ages (T_{DM2}) were calculated by assuming a mean $^{176}Lu/^{177}Hf$ value of 0.015 for the average continental crust (Vervoort and Blichert-Toft, 1999).Initial $^{176}Hf/^{177}Hf$ ratios and $\varepsilon_{Hf}(t)$ values are calculated by the zircon crystallization ages.

4.3. Whole rock major- and trace-element analysis

Fresh rock samples were crushed in a steel crusher and then powdered in an agate mill to a grain size <200 mesh for analyses. The major elements were analyzed by X-ray fluorescence (XRF) at the State Key lab of Biogeology and Environmental Geology, China University of Geosciences. The analytical uncertainty is better than 5%. Trace elements were measured using Agilent 7500a ICP–MS at the State Key Laboratory of Geological Processes and Mineral Resources (GPMR), China University of Geosciences, Wuhan. The detailed sample-digesting procedure for ICP–MS analyses and analytical precision and accuracy for trace elements are the same as described by Liu et al. (2008).

4.4. Measurements of Ti content in quartz

The measurements of Ti content in quartz were performed using OL-JXA-8100 electron microprobe at the GPMR. The accelerating voltage,

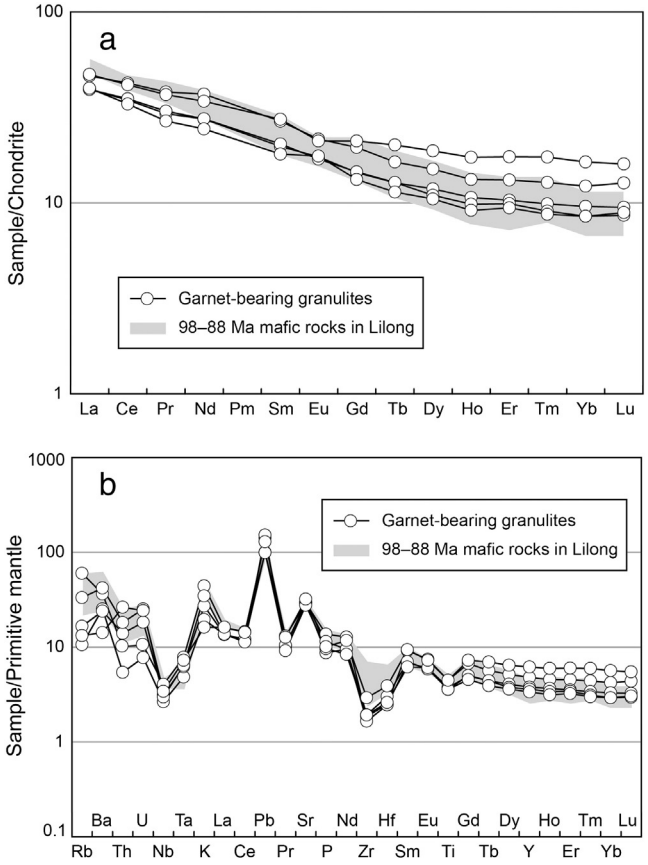

Fig. 7. Multi-element plots for Nyingchi Complex garnet-bearing granulite samples of this study compared with Lilong mafic rocks (data from Guan et al., 2011). (a) REE patterns normalized to chondrites; (b) Primitive mantle-normalized spider diagram. All normalization values from Sun and McDonough (1989).

Please cite this article as: Guo, L., et al., Late Cretaceous (~81 Ma) high-temperature metamorphism in the southeastern Lhasa terrane: Implication for the Neo-Tethys ocean ridge subduction, Tectonophysics (2013), http://dx.doi.org/10.1016/j.tecto.2013.10.007

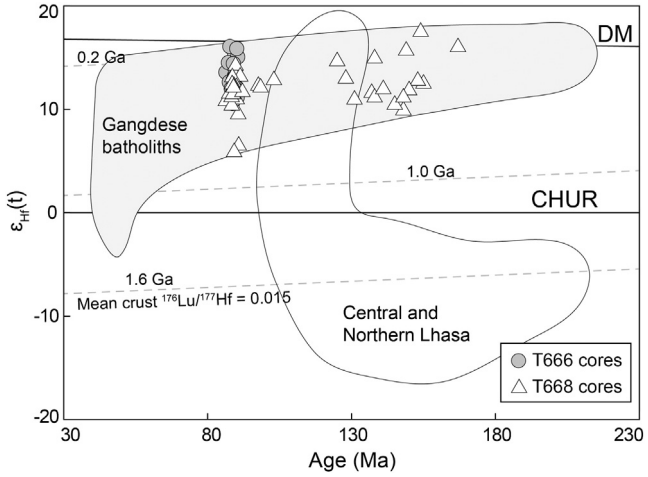

Fig. 8. Plots of $\varepsilon_{Hf}(t)$ values versus U–Pb ages of the magmatic zircons from the studied samples. Also plotted, for comparison, published magmatic zircon data of the Gangdese batholiths (Chu et al., 2006; Guan et al., 2010; Ji et al., 2009; Zhang et al., 2007; Zhu et al., 2011) and the Northern Lhasa terrane plutonic belt (Chu et al., 2006; Zhang et al., 2007; Zhu et al., 2009a, 2009b, 2011). CHUR = chondritic uniform reservoir; DM = depleted mantle.

beam current, and counting time were set to 15 kV, 20 nA, and 30 s, respectively.

5. Results

5.1. Zircon U–Pb geochronology and trace-element geochemistry

5.1.1. Garnet-bearing granulite

Zircons from sample T666 are subhedral or euhedral, with grain lengths of 200–500 μm and aspect ratios of 1:1–1:3. In CL images (Fig. 3a), most zircons exhibit core–rim structures. The cores show banded zoning and sector zoning with brighter luminescence than the rims, indicating that they are magmatic in origin (Corfu et al., 2003). The rims exhibit no zoning, and are interpreted as metamorphic overgrowths (Corfu et al., 2003). Thirty-six analyses on 22 zircon grains were carried out. Twenty-two analyses on the cores have Th of 39.6–202 ppm, U of 80.0–261 ppm, with Th/U ratios of 0.46–0.77 (mean = 0.62, Table A1). The magmatic cores are enriched in HREE, and have positive Ce anomalies and marked negative Eu anomalies (Eu/Eu* = 0.17–0.32) (Fig. 4a). They yield $^{206}Pb/^{238}U$ ages ranging from 86.5 to 92.5 Ma, with a weighted mean of 89.3 ± 0.6 Ma (MSWD = 0.97) (Fig. 5a; Table A2), representing the crystallization age of the protolith of the garnet-bearing granulite. The metamorphic rims have low Th/U ratios of 0.30–0.50 (except for the spot T666-05r, mean = 0.38) and low REE contents (Fig. 4a; Tables A1 and A2). They display HREE-enriched patterns with positive Ce anomalies and moderate negative Eu anomalies (Eu/Eu* = 0.40–0.82) (Fig. 4a), distinct from those of the magma zircons in this sample. The metamorphic rims yield $^{206}Pb/^{238}U$ ages of 80.5–81.8 Ma, with a weighted mean age of 81.1 ± 0.8 Ma (MSWD = 0.05) (Fig. 5a), which is interpreted as the metamorphic age.

5.1.2. Marble

The detrital zircons in sample T668 vary from euhedral to subrounded in shape, and range in size from 80 to 300 μm with aspect ratios of 1:1–1:3. The euhedral crystal shape implies relatively short transport distances prior to deposition. In CL images (Fig. 3b), most zircons exhibit core–rim structures. The cores show oscillatory zoning, indicating that they are magmatic zircons (Corfu et al., 2003). The rims display planar zoning or no zoning, which is typical of metamorphic origin (Corfu et al., 2003). Some grains show planar zoning or no zoning, similar to the metamorphic rims (Fig. 3b). Sixty-seven analyses on 67 zircon grains were carried out. Forty-eight analyses on the cores have Th of 17.0–1598 ppm, U of 124–4314 ppm, with Th/U ratios of 0.03–1.17 (Table A1). They are enriched in HREE, and have positive Ce anomalies and marked negative Eu anomalies (Eu/Eu* = 0.04–0.77) (Fig. 4b; Table A2). Their $^{206}Pb/^{238}U$ ages rang from 86.3 to 167 Ma, with two populations at 86–100 Ma and 120–155 Ma, respectively (Fig. 5b and c). The youngest age peak is 89.7 Ma (Fig. 5c), giving a maximum depositional age of the protolith. In contrast, nineteen analyses on the metamorphic domains have Th of 21.3–1591 ppm, U of 145.8–1023 ppm, with variable Th/U ratios of 0.12–1.56 (Table A1). They have relatively flat M-HREE patterns, and largely weak negative Eu anomaly (Eu/Eu* = 0.42–1.05) (Fig. 4b). This is also distinct from those of the cores in this sample. They have $^{206}Pb/^{238}U$ ages ranging from 80.4 Ma to 84.4 Ma, with a weighted mean of 81.4 ± 0.5 Ma (MSWD = 0.74) (Fig. 5b), which is interpreted as the metamorphic age.

5.2. Whole-rock geochemistry of the garnet-bearing granulite

Petrographic observation shows that the garnet-bearing granulite samples have experienced various degrees of alteration, as indicated by the presence of epidote and clinozoisite (Fig. 2). Some major elements (e.g., K and Na) and large-ion lithophile elements (LILE, e.g., Cs, Rb and Ba) could be mobilized during metamorphism and alteration (Chesworth et al., 1981; Wood et al., 1979). In contrast, high field-strength elements (HFSE, e.g., Nb, Ta, Zr, Hf, Ti, Y), REE and transitional elements (e.g., Ni, Cr, V, and Sc) are considered to be relatively immobile during alteration and metamorphism (Middelburg et al., 1988; Wood et al., 1979). We thus chose the relatively immobile elements to discuss the protolith nature of the garnet-bearing granulite.

Whole rock major- and trace-element data of the garnet-bearing granulite are presented in Table 1. All the studied samples show low LOI of 0.74–1.46% (Table 1), suggesting that they were not significantly

Table 2
Measured Ti contents in quartz and *T* (°C) estimation with TitaniQ thermometer.

Sample	Na_2O	K_2O	Cr_2O_3	MgO	CaO	MnO	Al_2O_3	TiO_2	FeO	SiO_2	ZrO_2	Total	Ti	T (°C)	
	w (%)												*ppm*	P = 10 kbar	P = 13 kbar
Spot = 50 μm															
T666-01	–*	–	–	0.003	0.008	–	0.058	0.029	0.024	99.252	–	99.374	174	821	894
T666-02	–	–	–	0.006	–	–	0.037	0.032	–	99.519	0.032	99.626	192	834	908
T666-03	–	–	–	–	–	0.014	0.050	0.035	–	99.769	–	99.868	210	846	920
T666-04	0.011	–	–	0.025	0.015	–	0.060	0.036	–	99.606	–	99.753	216	849	924
T666-05	0.003	–	–	0.020	0.029	0.027	0.038	0.035	–	99.380	–	99.532	210	846	920
T666-06	0.012	0.022	–	0.010	0.011	–	0.051	0.028	–	99.463	–	99.597	168	817	889
T666-07	–	0.002	0.005	0.026	0.002	–	0.056	0.027	0.021	99.502	–	99.641	162	812	885
T666-08	0.003	0.002	–	0.037	–	–	0.048	0.026	–	99.658	–	99.774	156	807	880
T666-09	–	–	–	0.016	–	–	0.041	0.035	–	99.611	–	99.703	210	846	920
T666-10	–	–	–	0.006	–	–	0.040	0.025	0.011	98.726	–	98.808	150	803	874

* Below detection limit.

Please cite this article as: Guo, L., et al., Late Cretaceous (~81 Ma) high-temperature metamorphism in the southeastern Lhasa terrane: Implication for the Neo-Tethys ocean ridge subduction, Tectonophysics (2013), http://dx.doi.org/10.1016/j.tecto.2013.10.007

carbonated during metamorphism and alteration. They have SiO_2 of 50.71–54.65%, and are characterized by high Al_2O_3 (16.73–19.54%), low TiO_2 (0.78–0.97%), low MgO (2.85–4.81%) and low Mg# of 33–51 (Table 1). Their protoliths are sub-alkaline basalts according to the Zr/TiO_2 – Nb/Y classification diagram (Winchester and Floyd, 1977) (Fig. 6a). In the Co – Th classification diagram, they plot in the calc-alkaline basalt field (Hastie et al., 2007) (Fig. 6b).

The chondrite-normalized REE patterns (Fig. 7a) show LREE enrichment [$(La/Yb)_N$ = 2.9–4.7] with Eu/Eu^* = 0.87–1.13. They are enriched in K, Pb and Sr, and depleted in Nb, Ta, Zr, Hf and Ti relative to their neighboring elements (Fig. 7b). These geochemical characteristics are similar to those of the Late Cretaceous (98–88 Ma) mafic rocks in Linlong area (Fig. 7) (Guan et al., 2011).

5.3. Isotope geochemistry

The whole-rock Sr – Nd isotopic composition for the garnet-bearing granulite samples is given in Table 1. Lu – Hf isotope analyses for zircon

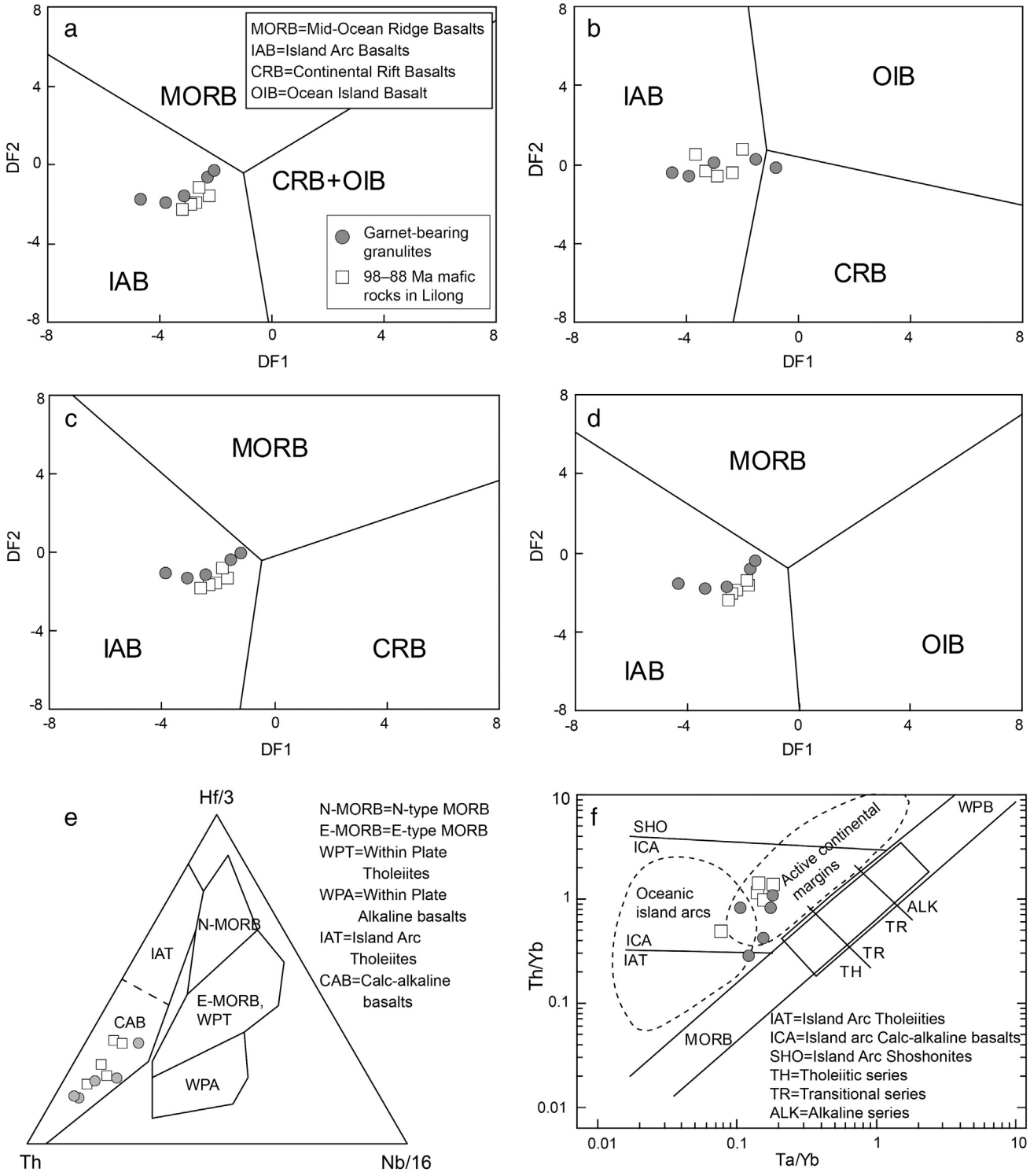

Fig. 9. Immobile trace-element tectonic discrimination diagrams for the garnet-bearing granulite. (a–d) The immobile trace element discriminant function tectonic setting diagram of Agrawal et al. (2008); (e) Hf/3-Th – Nb/16 (Wood, 1980); (f) Th/Yb – Ta/Yb (Pearce, 1982).

Please cite this article as: Guo, L., et al., Late Cretaceous (~81 Ma) high-temperature metamorphism in the southeastern Lhasa terrane: Implication for the Neo-Tethys ocean ridge subduction, Tectonophysics (2013), http://dx.doi.org/10.1016/j.tecto.2013.10.007

grains from the garnet-bearing granulite and the marble samples are presented in Table A3 and are plotted in Fig. 8.

The initial $^{87}Sr/^{86}Sr$ ratios and $\varepsilon_{Nd}(t)$ values are calculated at $t =$ 89 Ma. Four garnet-bearing granulite samples have relatively homogeneous initial $^{87}Sr/^{86}Sr$ ratios of 0.70433–0.70456 and positive $\varepsilon_{Nd}(t)$ values ranging from +2.7 to +4.6 (Table 1). Eighteen Hf isotopic analyses on the magmatic cores of the zircons from garnet-bearing granulite have $\varepsilon_{Hf}(t)$ values from +10.5 to +16.0, and two-stage model ages (T_{DM2}) from 126 to 479 Ma (Table A3 and Fig. 8). These values are similar to those of the mafic rocks (~88 Ma) in Lilong area, which show initial $^{87}Sr/^{87}Sr$ ratio of ~0.70427, $\varepsilon_{Nd}(t)$ value of +3.0, and $\varepsilon_{Hf}(t)$ values of +11.8 to +17.2 (Guan et al., 2011).

Thirty-eight Hf isotopic analyses on the magmatic cores of detrital zircons from the marble yield $\varepsilon_{Hf}(t)$ values ranging from +5.9 to +17.5, corresponding to the T_{DM2} of 82–778 Ma (Table A3 and Fig. 8).

5.4. Ti-in-quartz geothermometry

The quartz grains in the garnet-bearing granulite contain abundant exsolved rutile needles (Fig. 2f). Experimental studies have shown that the Ti contents in quartz increase with rising temperature and decrease with increasing pressure (Kawasaki and Osanai, 2008; Thomas et al., 2010; Wark and Watson, 2006). Hence exsolution is commonly a consequence of rutile nucleation in response to decreasing Ti solubility during cooling or decompression (Kawasaki and Osanai, 2008; Thomas et al., 2010; Wark and Watson, 2006). Wark and Watson (2006) experimentally calibrated the Ti-in-quartz (TitaniQ) thermometer based on the temperature dependence of Ti solubility in quartz. Thomas et al. (2010) further investigated the effect of pressure on the Ti-in-quartz solubility, and developed TitaniQ thermobarometer that enables estimations of the temperature and pressure conditions of igneous and metamorphic rocks when used in combination with independent thermobarometers. The TitaniQ temperature is determined using equation 12 of Thomas et al. (2010): $T(^{\circ}C) = \frac{60952+1741\cdot P(kbar)}{1.52-R\bar{n}\ \ln X_{TiO_2}^{Qtz}+R\bar{n}\ \ln a_{TiO_2}} - 273.15$, where P is the pressure (kbar), R is the gas constant (8.314472 J/K), $X_{TiO_2}^{Qtz}$ is the mole fraction of TiO_2 in quartz and a_{TiO_2} is the activity of TiO_2 in the system.

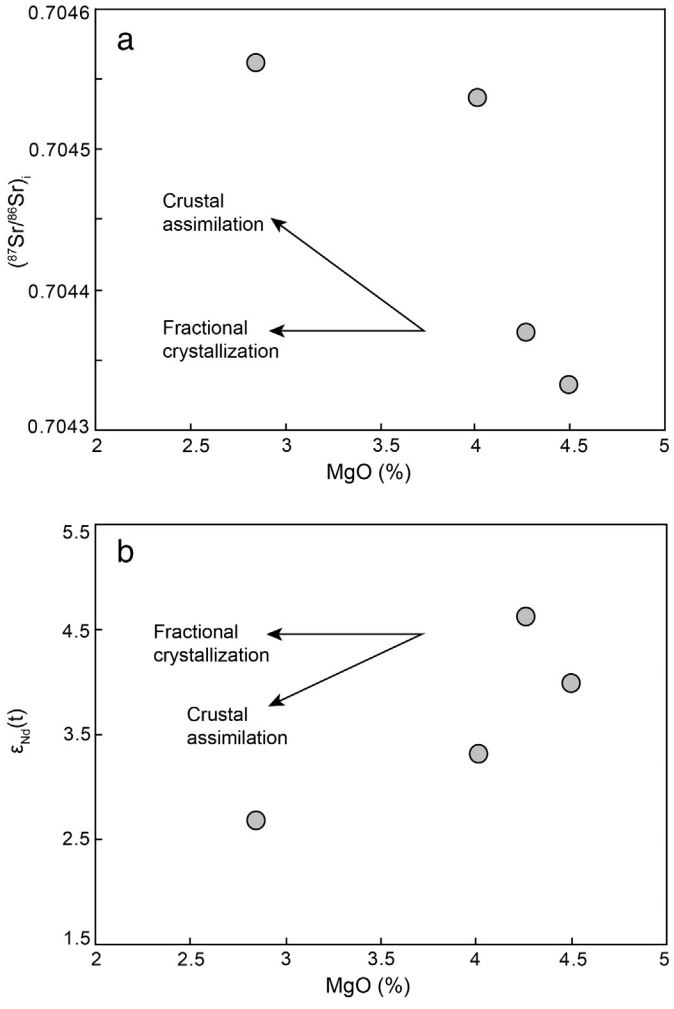

Fig. 10. (a) $(^{87}Sr/^{86}Sr)_i$ versus MgO, (b) $\varepsilon_{Nd}(t)$ versus MgO for the garnet-bearing granulites.

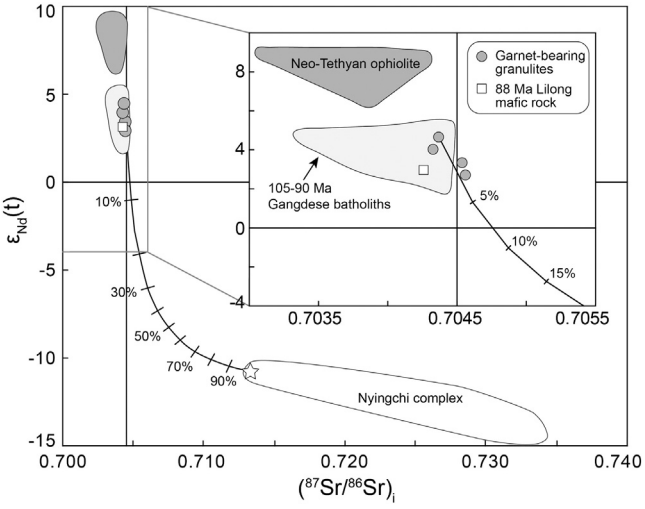

Fig. 11. $\varepsilon_{Nd}(t)$ versus $(^{87}Sr/^{86}Sr)_i$ diagram of the garnet-bearing granulites. Bulk-rock Sr – Nd isotopic ratios calculated at $t = 89$ Ma. Fields for the Neo-Tethyan ophiolites and Late Cretaceous (105–90 Ma) Gangdese batholiths taken from Wen et al. (2008a) and references therein. Data for the Lilong mafic rocks and the Nyingchi Complex are taken from Guan et al. (2010) and Zhang et al. (2010a), respectively. Garnet-bearing sample T667 and metasedimentary sample T527 in Nyingchi Complex (Zhang et al., 2010a) are used to model the mantle-derived and crustal end-member, respectively.

The analyzed quartz in this study contains fine, oriented needles of exsolved rutile spaced 10–20 μm apart (Fig. 2f). Rutile needles are distributed throughout the entire area of quartz grains (Fig. 2f), suggesting that Ti diffusion is insignificant. In order to obtain reliable Ti content of pre-exsolution quartz, we adopted the large-area-averaged method (Adachi et al., 2010; Wark and Watson, 2006) using a beam diameter of 50 μm. Ten analyses were performed on six quartz grains. The results show that the predominant trace elements present in quartz are Mg, Al and Ti (Table 2). The Ti contents range from 150 to 216 ppm (Table 2). Based on the presence of rutile throughout the prograde and retrograde metamorphic stages, the activity of titanium (a_{TiO_2}) is assumed to be 1. Considering that the peak metamorphic mineral assemblages for the garnet-bearing granulite are similar to those of the adjacent felsic granulite reported by Zhang et al. (2010c), we assumed a pressure of 10–13 kbar, obtained by conventional barometry (Zhang et al., 2010c), to calculate the peak metamorphic temperature. Our calculated results show that the metamorphic temperatures are 803–849 °C at $P =$ 10 kbar and 874–924 °C at $P = 13$ kbar (Table 1), consistent with the peak metamorphic temperatures of 830–900 °C, estimated by conventional thermometers (Zhang et al., 2010c).

6. Discussion

6.1. Petrogenesis of the garnet-bearing granulite and the marble

6.1.1. Garnet-bearing granulite

Late Cretaceous (110–80 Ma) Gangdese arc magmatism was widespread in the southern Lhasa terrane along the IYSZ (Guan et al.,

2011; Ji et al., 2009; Wen et al., 2008b). Guan et al. (2011) reported a suite of Late Cretaceous (98–88 Ma) mafic rocks in Lilong area, and suggested that they were formed from partial melting of the metasomatized mantle wedge. The protolith age (~89 Ma) of the garnet-bearing granulite is similar to the crystallization age (~88 Ma) of the Lilong mafic rocks (Sample ML24-2) (Guan et al., 2011). Both the garnet-bearing granulite and the Lilong mafic rocks have high Al_2O_3 (>16.7%), low MgO (Mg# = 33–51) and low TiO_2 (<1.1%) (Table 1). They are calc-alkaline (Fig. 6), and show LREE enrichment (Fig. 7a) and marked negative Nb, Ta, Zr, Hf and Ti anomalies (Fig. 7b). Those characteristics are typical of subduction-related magmas (Pearce and Peate, 1995). On the immobile trace element discriminant function tectonic setting diagrams (Agrawal et al., 2008), they all lie in the island arc basalt field (Fig. 9a–d). They further plot in the active continental margin arc field on the Hf/3-Th – Nb/16 (Fig. 9e) and Ta/Yb – Th/Yb (Fig. 9f) diagrams. The close spatial relationship (Fig. 1b) and their similarities in age and geochemical characteristics all strongly suggest that the protolith of the garnet-bearing granulites and the Lilong mafic rocks share a similar petrogenesis.

The garnet-bearing granulites have positive $\varepsilon_{Nd}(t)$ values of +2.7 to +4.6 (Table 1) and zircon $\varepsilon_{Hf}(t)$ values of +10.5 to +16.0 (Table A3 and Fig. 8), indicating that their protoliths were derived from a depleted mantle source. The negative correlation between MgO and $(^{87}Sr/^{86}Sr)_i$ (Fig. 10a) and positive correlation between MgO and $\varepsilon_{Nd}(t)$ (Fig. 10b) are consistent with crustal assimilation affecting the more evolved compositions. One potential crustal contaminant in the southeastern Lhasa terrane is provided by the Nyingchi Complex (Zhang et al., 2010a). The metasedimentary rocks in the Nyingchi Complex have negative $\varepsilon_{Nd}(t)$ values of −14.5 to −10.8 (for t = 89 Ma), and $(^{87}Sr/^{86}Sr)_i$ of 0.71330 to 0.73324 (Zhang et al., 2010a). From simple endmember modeling (Fig. 11), the protoliths of the garnet-bearing granulites can be generated by mixing of mantle derived magmas with a small amount (<5%) of crustal contaminants. The large $\varepsilon_{Hf}(t)$ variation (>5 units of $\varepsilon_{Hf}(t)$) of the 89 Ma zircons can account for such contamination (Kemp et al., 2007; Yang et al., 2007). On the basis of these observations, we suggest that the protolith of the garnet-bearing granulite was derived from partial melting of the mantle wedge, accompanied by small amounts of contamination by the Nyingchi Complex during magma ascent.

6.1.2. Marble

The magmatic cores of the detrital zircons from the marble yield $^{206}Pb/^{238}U$ ages of 86.3–167 Ma, and cluster at 86–100 Ma and 120–155 Ma, respectively (Fig. 5b, c). The youngest age peak defines a maximum depositional age of 89.7 Ma for the protolith of the marble (Fig. 6). Because the metamorphism occurred at 81.4 ± 0.5 Ma, the protolith must have been deposited between 90 and 81 Ma. Moreover, the age distribution of the detrital magmatic zircons in the marble matches well with the age spectra of the Jurassic–Cretaceous Gangdese batholiths and volcanic rocks (Chu et al., 2006; Guan et al., 2010, 2011; Guo et al., 2011, 2012; Ji et al., 2009; McDermid et al., 2002; Quidelleur et al., 1997; Wen et al., 2008b; Zhang et al., 2007, 2010b; Zhu et al., 2008, 2009a, 2009b, 2011) (Fig. 5c). They have positive $\varepsilon_{Hf}(t)$ values ranging from +5.9 to +17.5, indicating that their host rocks were derived from partial melting of juvenile crust or depleted mantle sources (Fig. 8), which is consistent with the characteristics of the Gangdese batholiths (Chu et al., 2006; Ji et al., 2009; Zhang et al., 2007). The euhedral crystal shape (Fig. 3b) suggests relatively short transport distances prior to deposition. The above observations strongly argue that the detrital zircons from the marble have been derived from erosion of the Gangdese batholiths and equivalent volcanic rocks. In addition, the detrital magmatic zircons have a similar age spectra to the Middle–Upper Cretaceous Xigaze forearc basin sedimentary rocks (Fig. 5c) (Aitchison et al., 2011; Wu et al., 2010). Considering the direct contact between the Nyingchi Complex and the Yarlung–Tsangpo suture zone (Fig. 1b), we propose that the protolith of the clastic component of the marble was deposited in the fore-arc basin of the Gangdese arc during Late Cretaceous.

6.2. The Late Cretaceous (~81 Ma) HT metamorphism

Our study indicates that the Nyingchi Complex underwent granulite-facies metamorphism, and was subsequently overprinted by amphibolite-facies retrograde metamorphism. The peak granulite-facies mineral assemblage is garnet + orthopyroxene + high-Ti amphibole + plagioclase + quartz + rutile (Fig. 2), which is similar to those of the adjacent felsic granulites in the Nyingchi Complex (Zhang et al., 2010c). The single rutile crystals contain regular ilmenite exsolution lamellae (Fig. 2g), indicating that they have high Fe content and formed during HT metamorphism (Banfield and Veblen, 1991; Zack et al., 2004). In addition, amphibole, garnet and quartz all contain abundant exsolved rutile needles (Fig. 2b, d, f), suggesting that their precursors have high Ti contents. The peak metamorphic temperatures estimated by using TitaniQ geothermometer are 803–924 °C (Table 2), which are consistent with the previous estimations for adjacent felsic granulite in the Nyingchi Complex (Zhang et al., 2010c).

All the inherited (magmatic and detrital) zircon cores of both the garnet-bearing granulite and the marble have similar chondrite-normalized REE patterns (Fig. 4). The REE patterns of inherited (magmatic and detrital) cores contain significantly higher REE contents than those of metamorphic rims. Their pronounced negative Eu anomaly, and positive Ce anomaly is a common feature of magmatic zircon (Hoskin and Schaltegger, 2003). The metamorphic zircon rims in the garnet-bearing granulite (sample T666) have relatively low Th/U ratios and low REE contents (Table A2). The REE patterns of the metamorphic zircon rims in garnet-bearing granulite show steep slopes from the HREE to LREE with moderately negative Eu anomalies ($Eu/Eu^* = 0.40 \sim 0.82$) and positive Ce anomalies (Fig. 4a). Enrichment of HREE indicates that the metamorphic zircon rims did not equilibrate with garnet in this sample, or formed in an "open" system situation with an infinite reservoir of trace element (Rubatto, 2002). The decreasing Eu anomaly, compared to the inherited magmatic zircons, is compatible with the release of Eu due to the break-down of minor plagioclase. The metamorphic rims/zircons in the marble (sample T668) have relatively flat M-HREE patterns, and weak negative Eu anomaly ($Eu/Eu^* = 0.42–1.05$) (Fig. 4b). Depletion of HREE indicates they grew during or after the crystallization of garnet. However, the lack of garnet in the marble (Fig. 2h) suggests that they probably formed in an "open" system. The weak negative Eu anomaly indicates that the metamorphic rims/zircons coexisted with minor or no feldspar. The geochemistry of the metamorphic rims/zircons in the garnet-bearing granulite and the marble suggests that they probably formed in an "open" system situation during the peak granulite-facies metamorphic stage. LA-ICP MS U – Pb zircon dating results show that they yield a consistent metamorphic age of ~81 Ma (Fig. 5a, b). We thus propose that the Nyingchi Complex experienced HT granulite-facies metamorphism at ~81 Ma.

6.3. Late Cretaceous Neo-Tethys oceanic ridge subduction

Our work demonstrates that the protolith of the garnet-bearing granulites is typical of continental margin arc rocks whereas the protolith of the marble formed in the fore-arc basin of the Gangdese arc. Typically the fore-arc region is characterized by low-temperature metamorphism resulting from the subduction of cold oceanic lithosphere (Groome and Thorkelson, 2009). However, in the southeastern Lhasa terrane both the arc magmatic rocks and fore-arc sedimentary rocks underwent HT granulite facies metamorphism at ~81 Ma. Therefore, the Late Cretaceous HT metamorphism requires a tectonic setting that allows an anomalously high heat flux in the fore-arc region. Several tectonic models may account for a high heat flux in such a setting, for example, slab break-off which is sometimes a

Please cite this article as: Guo, L., et al., Late Cretaceous (~81 Ma) high-temperature metamorphism in the southeastern Lhasa terrane: Implication for the Neo-Tethys ocean ridge subduction, Tectonophysics (2013), http://dx.doi.org/10.1016/j.tecto.2013.10.007

response to continental collision (Davies and von Blanckenburg, 1995). The India–Asian continental collision took place at 55 ± 10 Ma (de Sigoyer et al., 2000; Najman et al., 2010, and references therein). Many studies suggested that the break-off of the Neo-Tethyan oceanic slab occurred at ~50 Ma (Ji et al., 2009; Lee et al., 2009; Wen et al., 2008b), considerably later than the ~81 Ma HT metamorphism in the southeastern Lhasa terrane. A second possibility is ridge subduction which places hot sub-slab asthenospheric mantle beneath the base of the overlying plate resulting in HT/UHT metamorphism in the slab window at the roots of the arc and fore-arc and so produces anomalously high temperatures at shallow crustal depth (Brown, 1998; Santosh and Kusky, 2010).

We suggest that the Late Cretaceous (~81 Ma) HT metamorphism in the southeastern Lhasa terrane resulted from the subduction of the Neo-Tethys ocean ridge based on the following evidence: (1) The temporal and spatial variation of the Gangdese arc magmatism indicates that there is a gap in the period between 80 and 70 Ma (Fig. 5c) (Ji et al., 2009; Wen et al., 2008b). Although Volkmer (2010) attributed this gap to the formation of eclogitic lithospheric root resulting from shortening of the Lhasa terrane, this model conflicts with the

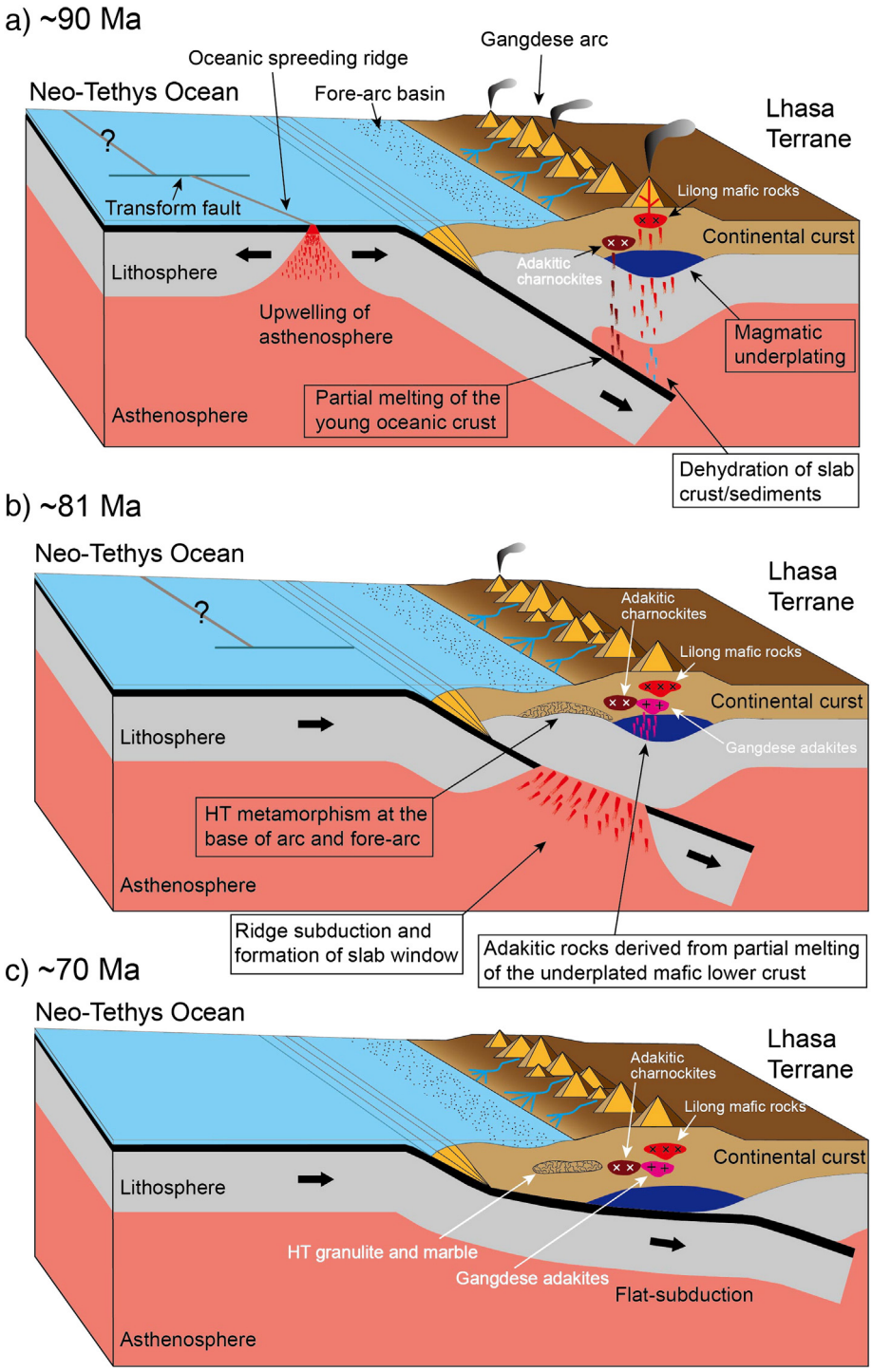

Fig. 12. Schematic tectonic model for of the evolution of the southern Lhasa terrane in the eastern Himalayan syntaxis area during 90–70 Ma. Details are in Section 6.4.

Please cite this article as: Guo, L., et al., Late Cretaceous (~81 Ma) high-temperature metamorphism in the southeastern Lhasa terrane: Implication for the Neo-Tethys ocean ridge subduction, Tectonophysics (2013), http://dx.doi.org/10.1016/j.tecto.2013.10.007

contemporary HT metamorphism recorded in the Nyingchi Complex (Zhang et al., 2010c; this study); (2) Wen et al. (2008a) reported a suite of epidote-bearing adakitic rocks (80–82 Ma) in the southeastern Lhasa terrane, and suggested that these rocks originated from partial melting of underplated mafic lower crust; (3) Guo et al. (2011) reported a Late Cretaceous granite (~81 Ma) which resulted from binary mixing between juvenile crustal materials (or mantle-derived magma) and an old crustal component, suggesting crustal anatexis at that time; (4) A major regional unconformity across southern Lhasa terrane has been documented, with gently dipping Palaeocene Linzizong volcanic rocks above folded Late Cretaceous and/or older rocks, showing that significant crustal uplift occurred prior to the India–Asia collision (Burg and Chen, 1984; England and Searle, 1986; Kapp et al., 2007; Leier et al., 2007); and (5) Gahalaut and Kundu (2012) analyzed the Gangdese arc morphology and earthquake ruptures, and suggested that the buoyant seismic/aseismic ridge subduction influenced the Gangdese arc morphology by causing a cusp in the southeastern Lhasa terrane. Taking all these independent and diverse studies into account, we propose that Late Cretaceous tectonothermal phenomena (the magmatic gap, adakitic rocks, crustal anatexis, fore-arc HT metamorphism, crustal uplift) were strongly influenced by the subduction of a Neo-Tethys oceanic ridge.

6.4. Late Cretaceous tectonic evolution of the southeastern Lhasa terrane

In order to explain the petrogenesis of the different rock types in the southeastern Lhasa terrane we propose a three-stage tectonic model accounting for the evolution of the southern Lhasa terrane during the Late Cretaceous, involving a stage of ridge subduction at ~81 Ma (Fig. 12). We do not propose a specific type of triple junction configuration in our model because of the lack of robust constraints on such speculation.

Stage 1 (~90 Ma): The young Neo-Tethys oceanic slab subducted beneath the Lhasa terrane prior to the arrival of the Neo-Tethys ridge at the trench (Fig. 12a). Dehydration of the down-going slab triggered partial melting of the mantle wedge to produce normal arc magmatism (Guan et al., 2011; this study). Contemporaneous melting of young, hot subducting oceanic crust resulted in the formation of adakitic charnockites (Zhang et al., 2010b). In the fore-arc basin, the detrital sediments were mainly derived from the erosion of the Gangdese batholiths and equivalent volcanic rocks (Fig. 12a).

Stage 2 (~81 Ma): The Neo-Tethys ocean ridge entered the trench (Fig. 12b). The resulting slab window placed the sub-slab asthenospheric mantle beneath the base of the overlying southern Lhasa terrane, which resulted in HT metamorphism in the roots of the arc and fore-arc basin (Brown, 1998; Santosh and Kusky, 2010). High heat flow through the slab window further induced partial melting of overlying crustal rocks to form intermediate to acidic magmas, which included adakitic magma sourced from partial melting of the newly underplated mafic lower crust (Guan et al., 2010; Wen et al., 2008a), and granitic magma derived from mixing of juvenile and older crustal materials (Guo et al., 2011). In addition, the early uplift of the southern Lhasa terrane was triggered by subduction of the Neo-Tethys ocean ridge due to its topography and buoyancy, resulting in contraction and uplift in the overlying fore-arc (Guillaume et al., 2009, 2010). The influx of asthenospheric mantle through the slab window may have enhanced early uplift of the southern Lhasa terrane (Guillaume et al., 2010; Zandt and Humphreys, 2008). This provides an explanation for the cessation of deposition of the Takena Formation, which was deposited in a retroarc foreland basin, and its subsequent uplift, deformation and erosion during Late Cretaceous (Leier et al., 2007).

Stage 3 (~70 Ma): Following ridge subduction, the young, warm, and thus buoyant oceanic slab subducted beneath the southern Lhasa terrane (Fig. 12c), which induced transient shallow subduction (Gutscher et al., 2000; Wen et al., 2008a). Contractional deformation occurred in the upper plate, and crustal thickening occurred in the arc–backarc region (Collins, 2002; Gutscher et al., 2000).

7. Conclusions

This study of a garnet-bearing granulite and a marble from the Nyingchi Complex of the southeastern Lhasa terrane documents high-temperature, granulite-facies metamorphism and subsequent amphibolite-facies retrograde metamorphism. The granulite-facies assemblage is characterized by garnet + orthopyroxene + high-Ti amphibole + plagioclase + quartz + rutile. The amphibole, garnet, quartz grains contain abundant of exsolved rutile needles, suggesting that their precursors had high Ti contents. The peak metamorphic temperature is 803–924 °C estimated using the TitaniQ geothermometer. Whole rock major and trace elements and Sr – Nd – Hf isotopic compositions, together with isotopic studies of zircons indicate that their protoliths were island-arc basaltic rocks that had crystallized at 89.3 ± 0.6 Ma. The detrital magmatic zircons from the marble have a similar age distribution and $\varepsilon_{Hf}(t)$ values to those of the Jurassic–Cretaceous Gangdese batholiths and volcanic rocks, suggesting that the detritus has been derived from the Gangdese batholiths or equivalent volcanic rocks, and deposited in the forearc basin. The metamorphic zircons in the garnet-bearing granulite and marble yield a consistent metamorphic age of ~81 Ma. This event was coeval with a hiatus in arc magmatism, a regional unconformity and with crustal anatexis. We propose that the HT metamorphism resulted from the Neo-Tethys ocean ridge subduction in the southeastern Lhasa terrane.

Supplementary data to this article can be found online at http://dx.doi.org/10.1016/j.tecto.2013.10.007.

Acknowledgments

This research is supported by the National Key Project for Basic Research (no. 2011CB403102), the Natural Science Foundation of China (grants: 41073046 and 41103019), China Geological Survey (no. 1212011121261), SinoProbe 04-02, and the Fundamental Research Funds for the Central Universities, China University of Geosciences (Wuhan). L. Guo thanks F. Shi and Y.-F. Zhang for help with preparation of thin section. We also thank Prof. R.B. Cole and an anonymous reviewer for their constructive comments that greatly improved this manuscript.

References

Adachi, T., et al., 2010. Titanium behavior in quartz during retrograde hydration: Occurrence of rutile exsolution and implications for metamorphic processes in the Sør Rondane Mountains, East Antarctica. Polar Sci. 3, 222–234.
Agrawal, S., Guevara, M., Verma, S.P., 2008. Tectonic discrimination of basic and ultrabasic volcanic rocks through log-transformed ratios of immobile trace elements. Int. Geol. Rev. 50, 1057–1079.
Aguillon-Robles, A., et al., 2001. Late miocene adakites and Nb-enriched basalts from Vizcaino Peninsula, Mexico: indicators of East Pacific Rise subduction below Southern Baja California? Geology 29, 531–534.
Aitchison, J.C., Xia, X., Baxter, A.T., Ali, J.R., 2011. Detrital zircon U – Pb ages along the Yarlung–Tsangpo suture zone, Tibet: Implications for oblique convergence and collision between India and Asia. Gondwana Res. 20, 691–709.
Allègre, C.J., et al., 1984. Structure and evolution of the Himalaya–Tibet Orogenic Belt. Nature 307, 17–22.
Banfield, J.F., Veblen, D.R., 1991. The structure and origin of Fe-bearing platelets in metamorphic rutile. Am. Mineral. 76, 113–127.
Blichert-Toft, J., Albarede, F., 1997. The Lu – Hf isotope geochemistry of chondrites and the evolution of the mantle–crust system. Earth Planet. Sci. Lett. 148, 243–258.
Booth, A.L., Chamberlain, C.P., Kidd, W.S.F., Zeitler, P.K., 2009. Constraints on the metamorphic evolution of the eastern Himalayan syntaxis from geochronologic and petrologic studies of Namche Barwa. Geol. Soc. Am. Bull. 121, 385–407.
Bradley, D.C., et al., 2003. Geologic signature of early Tertiary ridge subduction in Alaska. Geol. Soc. Am. Spec. Pap. 371, 19–49.
Brown, M., 1998. Ridge-trench interactions and high-T-low-P metamorphism, with particular reference to the Cretaceous evolution of the Japanese Islands. Geol. Soc. Lond. Spec. Publ. 138, 137–169.
Burg, J.P., Chen, G.M., 1984. Tectonics and structural zonation of southern Tibet, China. Nature 311, 219–223.

Please cite this article as: Guo, L., et al., Late Cretaceous (~81 Ma) high-temperature metamorphism in the southeastern Lhasa terrane: Implication for the Neo-Tethys ocean ridge subduction, Tectonophysics (2013), http://dx.doi.org/10.1016/j.tecto.2013.10.007

Chesworth, W., Dejou, J., Larroque, P., 1981. The weathering of basalt and relative mobilities of the major elements at Belbex, France. Geochim. Cosmochim. Acta 45, 1235–1243.

Chu, M.F., et al., 2006. Zircon U–Pb and Hf isotope constraints on the Mesozoic tectonics and crustal evolution of southern Tibet. Geology 34, 745–748.

Cole, R.B., Stewart, B.W., 2009. Continental margin volcanism at sites of spreading ridge subduction: Examples from southern Alaska and western California. Tectonophysics 464, 118–136.

Cole, R.B., Nelson, S.W., Layer, P.W., Oswald, P.J., 2006. Eocene volcanism above a depleted mantle slab window in southern Alaska. Geol. Soc. Am. Bull. 118, 140–158.

Collins, W.J., 2002. Hot orogens, tectonic switching, and creation of continental crust. Geology 30, 535–538.

Corfu, F., Hanchar, J.M., Hoskin, P.W.O., Kinny, P., 2003. Atlas of zircon textures. Rev. Mineral. Geochem. 53, 469–500.

Coulon, C., Maluski, H., Bollinger, C., Wang, S., 1986. Mesozoic and Cenozoic Volcanic rocks from Central and Southern Tibet: $^{39}Ar-^{40}Ar$ dating, petrological characteristics and geodynamical significance. Earth Planet. Sci. Lett. 79, 281–302.

Davies, J.H., von Blanckenburg, F., 1995. Slab breakoff: a model of lithosphere detachment and its test in the magmatism and deformation of collisional orogens. Earth Planet. Sci. Lett. 129, 85–102.

de Sigoyer, J., et al., 2000. Dating the Indian continental subduction and collisional thickening in the northwest Himalaya: Multichronology of the Tso Morari eclogites. Geology 28, 487–490.

DeLong, S.E., Schwarz, W.M., Anderson, R.N., 1979. Thermal effects of ridge subduction. Earth Planet. Sci. Lett. 44, 239–246.

Dewey, J.F., Shackleton, R.M., Chengfa, C., Yiyin, S., 1988. The tectonic evolution of the Tibetan Plateau. Philosophical transactions of the Royal Society of London. Ser. A Math. Phys. Sci. 327, 379–413.

Dong, X., Zhang, Z., Santosh, M., 2010. Zircon U–Pb chronology of the Nyingtri Group, Southern Lhasa Terrane, Tibetan Plateau: implications for Grenvillian and Pan-African Provenance and Mesozoic–Cenozoic metamorphism. J. Geol. 118, 677–690.

Dong, X., et al., 2012. Genesis of the metamorphic rock from southeastern Lhasa terrane and the Mesozoic–Cenozoic orogenesis. Acta Petrol. Sin. 28, 1765–1784 (in Chinese with English abstract).

Dürr, S.B., 1996. Provenance of Xigaze fore-arc basin clastic rocks (Cretaceous, south Tibet). Geol. Soc. Am. Bull. 108, 669–684.

Einsele, G., et al., 1994. The Xigaze forearc basin: evolution and facies architecture (Cretaceous, Tibet). Sediment. Geol. 90, 1–32.

England, P., Searle, M., 1986. The Cretaceous-tertiary deformation of the Lhasa Block and its implications for crustal thickening in Tibet. Tectonics 5, 1–14.

Gahalaut, V.K., Kundu, B., 2012. Possible influence of subducting ridges on the Himalayan arc and on the ruptures of great and major Himalayan earthquakes. Gondwana Res. 21, 1080–1088.

Geng, Q.R., et al., 2006. The Eastern Himalayan syntaxis: major tectonic domains, ophiolitic melanges and geologic evolution. J. Asian Earth Sci. 27, 265–285.

Geng, Q., Peng, Z., Zhang, Z., 2010. Geochemical study on metamorphosed mafic rocks in ophiolitic zone in the Yarlung Zangpo Great Bend, eastern Tibet, China. Geol. Bull. China 29, 1781–1794 (in Chinese with English abstract).

Geng, Q., Peng, Z., Zhang, Z., 2011. Geochronological study of the Yarlung Tsangpo ophiolite in the region of the eastern Himalayan syntaxis. Acta Geol. Sin. 85, 1116–1127 (in Chinese with English abstract).

Griffin, W.L., et al., 2000. The Hf isotope composition of cratonic mantle: LAM-MC-ICPMS analysis of zircon megacrysts in kimberlites. Geochim. Cosmochim. Acta 64, 133–147.

Groome, W.G., Thorkelson, D.J., 2009. The three-dimensional thermo-mechanical signature of ridge subduction and slab window migration. Tectonophysics 464, 70–83.

Guan, Q., et al., 2010. Late Cretaceous adakites in the eastern segment of the Gangdese Belt, southern Tibet: Products of Neo-Tethyan ridge subduction? Acta Petrol. Sin. 26, 2165–2179 (in Chinese with English abstract).

Guan, Q., et al., 2011. Zircon U–Pb chronology, geochemistry of the Late Cretaceous mafic magmatism in the southern Lhasa Terrane and its implications. Acta Petrol. Sin. 27, 2083–2094 (in Chinese with English abstract).

Guillaume, B., Martinod, J., Husson, L., Roddaz, M., Riquelme, R., 2009. Neogene uplift of central eastern Patagonia: dynamic response to active spreading ridge subduction? Tectonics 28 (TC2009).

Guillaume, B., Moroni, M., Funiciello, F., Martinod, J., Faccenna, C., 2010. Mantle flow and dynamic topography associated with slab window opening: Insights from laboratory models. Tectonophysics 496, 83–98.

Guo, L., Zhang, H.-F., Harris, N., Pan, F.-B., Xu, W.-C., 2011. Origin and evolution of multi-stage felsic melts in eastern Gangdese belt: Constraints from U–Pb zircon dating and Hf isotopic composition. Lithos 127, 54–67.

Guo, L., et al., 2012. Paleogene crustal anatexis and metamorphism in Lhasa terrane, eastern Himalayan syntaxis: evidence from U–Pb zircon ages and Hf isotopic compositions of the Nyingchi Complex. Gondwana Res. 21, 100–111.

Gutscher, M.A., Spakman, W., Bijwaard, H., Engdahl, E.R., 2000. Geodynamics of flat subduction: seismicity and tomographic constraints from the Andean margin. Tectonics 19, 814–833.

Haeussler, P.J., Bradley, D., Goldfarb, R., Snee, L., Taylor, C., 1995. Link between ridge subduction and gold mineralization in Southern Alaska. Geology 23, 995–998.

Harris, N.B.W., Holland, T.J.B., Tindle, A.G., 1988. Metamorphic rocks of the 1985 Tibet Geotraverse, Lhasa to Golmud. philosophical transactions of the Royal Society of London. Ser. A Math. Phys. Sci 327, 203–213.

Hastie, A.R., Kerr, A.C., Pearce, J.A., Mitchell, S.F., 2007. Classification of altered volcanic island arc rocks using immobile trace elements: development of the Th–Co discrimination diagram. J. Petrol. 48, 2341–2357.

Hoskin, P.W.O., Schaltegger, U., 2003. The composition of zircon and igneous and metamorphic petrogenesis. Rev. Mineral. Geochem. 53, 27–62.

Hu, D.G., et al., 2005. SHRIMP zircon U–Pb age and Nd isotopic study on the Nyainqentanglha Group in Tibet. Sci. China. Ser. D Earth Sci. 48, 1377–1386.

Hu, Z.C., et al., 2008. Signal enhancement in laser ablation ICP-MS by addition of nitrogen in the central channel gas. J. Anal. At. Spectrom. 23, 1093–1101.

Ji, W.Q., Wu, F.Y., Chung, S.L., Li, J.X., Liu, C.Z., 2009. Zircon U–Pb geochronology and Hf isotopic constraints on petrogenesis of the Gangdese batholith, southern Tibet. Chem. Geol. 262, 229–245.

Jiang, Z.-Q., Wang, Q., Li, Z.-X., Wyman, D.A., Tang, G.-J., Jia, X.-H., Yang, Y.-H., 2012. Late Cretaceous (ca. 90 Ma) adakitic intrusive rocks in the Kelu area, Gangdese Belt (southern Tibet): Slab melting and implications for Cu–Au mineralization. Journal of Asian Earth Sciences 53, 67–81.

Kapp, P., et al., 2007. The Gangdese retroarc thrust belt revealed. GSA Today 17, 4–9.

Kawasaki, T., Osanai, Y., 2008. Empirical thermometer of TiO_2 in quartz for ultrahigh-temperature granulites of East Antarctica. Geol. Soc. Lond. Spec. Publ. 308, 419–430.

Kemp, A.I.S., et al., 2007. Magmatic and crustal differentiation history of granitic rocks from Hf–O isotopes in zircon. Science 315, 980–983.

Lagabrielle, Y., et al., 2000. Magmatic–tectonic effects of high thermal regime at the site of active ridge subduction: the Chile Triple Junction model. Tectonophysics 326, 255–268.

Lee, H.Y., et al., 2009. Eocene Neotethyan slab breakoff in southern Tibet inferred from the Linzizong volcanic record. Tectonophysics 477, 20–35.

Leier, A.L., DeCelles, P.G., Kapp, P., Ding, L., 2007. The takena formation of the Lhasa terrane, southern Tibet: the record of a Late Cretaceous retroarc foreland basin. Geol. Soc. Am. Bull. 119, 31–48.

Liu, Y.S., et al., 2008. In situ analysis of major and trace elements of anhydrous minerals by LA-ICP-MS without applying an internal standard. Chem. Geol. 257, 34–43.

Liu, Y.S., et al., 2010a. Continental and oceanic crust recycling-induced melt-peridotite interactions in the Trans-North China Orogen: U–Pb dating, Hf isotopes and trace elements in zircons from mantle xenoliths. J. Petrol. 51, 537–571.

Liu, Y.S., et al., 2010b. Reappraisement and refinement of zircon U–Pb isotope and trace element analyses by LA-ICP-MS. Chin. Sci. Bull. 55, 1535–1546.

Ludwig, K.R., 2003. User's manual for Isoplot 3.0: a geochronological toolkit for Microsoft Excel. Berkeley Geochronology Center Special Publication, No.4.

Marshak, R.S., Karig, D.E., 1977. Triple junctions as a cause for anomalously near-trench igneous activity between the trench and volcanic arc. Geology 5, 233–236.

McCrory, P.A., Wilson, D.S., Stanley, R.G., 2009. Continuing evolution of the Pacific-Juan de Fuca-North America slab window system — a trench-ridge-transform example from the Pacific Rim. Tectonophysics 464, 30–42.

McDermid, I.R.C., Aitchison, J.C., Davis, A.M., Harrison, T.M., Grove, M., 2002. The Zedong terrane: a Late Jurassic intra-oceanic magmatic arc within the Yarlung–Tsangpo suture zone, southeastern Tibet. Chem. Geol. 187, 267–277.

Meng, F.Y., et al., 2010. Petrogenesis of Late Cretaceous adakite-like rocks in Mamba from the eastern Gangdese, Tibet. Acta Petrol. Sin. 26, 2180–2192 (in Chinese with English abstract).

Middelburg, J.J., van der Weijden, C.H., Woittiez, J.R.W., 1988. Chemical processes affecting the mobility of major, minor and trace elements during weathering of granitic rocks. Chem. Geol. 68, 253–273.

Najman, Y., et al., 2010. Timing of India–Asia collision: geological, biostratigraphic, and palaeomagnetic constraints. J. Geophys. Res. Solid Earth 115 B12416.

Nelson, E.P., Forsythe, R.D., 1989. Ridge collision at convergent margins: implications for Archean and post-Archean crustal growth. Tectonophysics 161, 307–315.

Pan, G., et al., 2012. Tectonic evolution of the Qinghai–Tibet Plateau. J. Asian Earth Sci. 53, 3–14.

Pavlis, T.L., Sisson, V.B., 1995. Structural history of the Chugach metamorphic complex in the Tana River region, eastern Alaska: a record of Eocene ridge subduction. Geol. Soc. Am. Bull. 107, 1333–1355.

Pearce, J.A., 1982. Trace element characteristics of lavas from destructive plate boundaries. In: Thorpe, R.S. (Ed.), Orogenic andesites and related rocks. John Wiley and Sons, Chichester, England, pp. 528–548.

Pearce, J.A., Peate, D.W., 1995. Tectonic Implications of the Composition of Volcanic Arc Magmas. Annu. Rev. Earth Planet. Sci. 23, 251–285.

Quidelleur, X., et al., 1997. Thermal evolution and slip history of the Renbu Zedong Thrust, southeastern Tibet. J. Geophys. Res. Solid Earth 102, 2659–2679.

Rogers, R.D., Karason, H., van der Hilst, R.D., 2002. Epeirogenic uplift above a detached slab in northern Central America. Geology 30, 1031–1034.

Rubatto, D., 2002. Zircon trace element geochemistry: partitioning with garnet and the link between U–Pb ages and metamorphism. Chem. Geol. 184, 123–138.

Santosh, M., Kusky, T., 2010. Origin of paired high pressure-ultrahigh-temperature orogens: a ridge subduction and slab window model. Terra Nova 22, 35–42.

Schärer, U., Xu, R.H., Allègre, C.J., 1984. U–Pb Geochronology of Gangdese (Transhimalaya) Plutonism in the Lhasa-Xigaze Region, Tibet. Earth Planet. Sci. Lett. 69, 311–320.

Scherer, E., Munker, C., Mezger, K., 2001. Calibration of the Lutetium–Hafnium Clock. Science 293, 683–687.

Sisson, V.B., Pavlis, T.L., Roeske, S.M., Thorkelson, D.J., 2003. Introduction: An overview of ridge-trench interactions in modern and ancient settings. Geol. Soc. Am. Spec. Pap. 371, 1–18.

Sun, S.-s, McDonough, W.F., 1989. Chemical and isotopic systematics of oceanic basalts: implications for mantle composition and processes. Geol. Soc. Lond. Spec. Publ. 42, 313–345.

Sun, W.D., et al., 2010. Ridge subduction and porphyry copper–gold mineralization: An overview. Sci. China Earth Sci. 53, 475–484.

Tang, G., et al., 2010. Ridge subduction and crustal growth in the Central Asian Orogenic Belt: Evidence from Late Carboniferous adakites and high-Mg diorites in the western Junggar region, northern Xinjiang (west China). Chem. Geol. 277, 281–300.

Thomas, J., et al., 2010. TitaniQ under pressure: the effect of pressure and temperature on the solubility of Ti in quartz. Contrib. Mineral. Petrol. 160, 743–759.

Please cite this article as: Guo, L., et al., Late Cretaceous (~81 Ma) high-temperature metamorphism in the southeastern Lhasa terrane: Implication for the Neo-Tethys ocean ridge subduction, Tectonophysics (2013), http://dx.doi.org/10.1016/j.tecto.2013.10.007

Thorkelson, D.J., 1996. Subduction of diverging plates and the principles of slab window formation. Tectonophysics 255, 47–63.
Thorkelson, D.J., Breitsprecher, K., 2005. Partial melting of slab window margins: genesis of adakitic and non-adakitic magmas. Lithos 79, 25–41.
Vervoort, J.D., Blichert-Toft, J., 1999. Evolution of the depleted mantle: Hf isotope evidence from juvenile rocks through time. Geochim. Cosmochim. Acta 63, 533–556.
Volkmer, J.E., 2010. The Cretaceous–Tertiary tectonic evolution of the Lhasa Terrane, Tibet. The University of Arizona (PhD. Thesis).
Wang, J.L., et al., 2009. Discovery of Late Cretaceous garnet two-pyroxene granulite in the southern Lhasa terrane, Tibet and its tectonic significances. Acta Petrol. Sin. 1695–1706 (in Chinese with English abstract).
Wark, D.A., Watson, E.B., 2006. TitaniQ: a titanium-in-quartz geothermometer. Contrib. Mineral. Petrol. 152, 743–754.
Wen, D.R., et al., 2008a. Late Cretaceous Gangdese intrusions of adakitic geochemical characteristics, SE Tibet: Petrogenesis and tectonic implications. Lithos 105, 1–11.
Wen, D.R., et al., 2008b. Zircon SHRIMP U–Pb ages of the Gangdese Batholith and implications for Neotethyan subduction in southern Tibet. Chem. Geol. 252, 191–201.
Winchester, J.A., Floyd, P.A., 1977. Geochemical discrimination of different magma series and their differentiation products using immobile elements. Chem. Geol. 20, 325–343.
Wood, D.A., 1980. The application of a Th-Hf-Ta diagram to problems of tectonomagmatic classification and to establishing the nature of crustal contamination of basaltic lavas of the British Tertiary Volcanic Province. Earth and Planetary Science Letters 50, 11–30.
Wood, D.A., Joron, J.-L., Treuil, M., 1979. A re-appraisal of the use of trace elements to classify and discriminate between magma series erupted in different tectonic settings. Earth Planet. Sci. Lett. 45, 326–336.
Wu, F.Y., Ji, W.Q., Liu, C.Z., Chung, S.L., 2010. Detrital zircon U–Pb and Hf isotopic data from the Xigaze fore-arc basin: Constraints on Transhimalayan magmatic evolution in southern Tibet. Chem. Geol. 271, 13–25.
Xu, R.H., Scharer, U., Allégre, C.J., 1985. Magmatism and Metamorphism in the Lhasa Block (Tibet): a Geochronological Study. J. Geol. 93, 41–57.
Yang, J.H., et al., 2007. Tracing magma mixing in granite genesis: in situ U–Pb dating and Hf-isotope analysis of zircons. Contrib. Mineral. Petrol. 153, 177–190.
Yin, A., Harrison, T.M., 2000. Geologic evolution of the Himalayan–Tibetan orogen. Annu. Rev. Earth Planet. Sci. 28, 211–280.
Yuan, H.L., et al., 2008. Simultaneous determinations of U–Pb age, Hf isotopes and trace element compositions of zircon by excimer laser-ablation quadrupole and multiple-collector ICP-MS. Chem. Geol. 247, 100–118.
Zack, T., Moraes, R., Kronz, A., 2004. Temperature dependence of Zr in rutile: empirical calibration of a rutile thermometer. Contrib. Mineral. Petrol. 148, 471–488.
Zandt, G., Humphreys, E., 2008. Toroidal mantle flow through the western U.S. slab window. Geology 36, 295–298.
Zhang, H.F., et al., 2007. Zircon U–Pb and Hf isotopic composition of deformed granite in the southern margin of the Gangdese belt, Tibet: Evidence for early Jurassic subduction of Neo-Tethyan oceanic slab. Acta Petrol. Sin. 23, 1347–1353.
Zhang, H.F., Xu, W.C., Zong, K.Q., Yuan, H.L., Harris, N., 2008. Tectonic evolution of metasediments from the Gangdise terrane, Asian plate, Eastern Himalayan Syntaxis, Tibet. Int. Geol. Rev. 50, 914–930.
Zhang, H., Harris, N., Guo, L., Xu, W., 2010a. The significance of Cenozoic magmatism from the western margin of the eastern syntaxis, southeast Tibet. Contrib. Mineral. Petrol. 160, 83–98.
Zhang, Z., et al., 2010b. Late Cretaceous charnockite with adakitic affinities from the Gangdese batholith, southeastern Tibet: Evidence for Neo-Tethyan mid-ocean ridge subduction? Gondwana Res. 17, 615–631.
Zhang, Z.M., et al., 2010c. Two stages of granulite facies metamorphism in the eastern Himalayan syntaxis, south Tibet: petrology, zircon geochronology and implications for the subduction of Neo-Tethys and the Indian continent beneath Asia. J. Metamorph. Geol. 28, 719–733.
Zhu, D.C., et al., 2008. SHRIMP zircon age and geochemical constraints on the origin of lower Jurassic volcanic rocks from the Yeba formation, Southern Gangdese, south Tibet. Int. Geol. Rev. 50, 442–471.
Zhu, D.C., et al., 2009a. Geochemical investigation of Early Cretaceous igneous rocks along an east–west traverse throughout the central Lhasa Terrane, Tibet. Chem. Geol. 268, 298–312.
Zhu, D.C., et al., 2009b. Early cretaceous subduction-related adakite-like rocks of the Gangdese Belt, southern Tibet: Products of slab melting and subsequent melt-peridotite interaction? J. Asian Earth Sci. 34, 298–309.
Zhu, D.-C., et al., 2011. The Lhasa Terrane: Record of a microcontinent and its histories of drift and growth. Earth Planet. Sci. Lett. 301, 241–255.

Please cite this article as: Guo, L., et al., Late Cretaceous (~81 Ma) high-temperature metamorphism in the southeastern Lhasa terrane: Implication for the Neo-Tethys ocean ridge subduction, Tectonophysics (2013), http://dx.doi.org/10.1016/j.tecto.2013.10.007